Journal of Computational Physics 228 (2009) 4248–4272

Contents lists available at ScienceDirect

Journal of Computational Physics

journal homepage: www.elsevier.com/locate/jcp

A systematic methodology for constructing high-order energy stable WENO schemes

Nail K. Yamaleev [a,*], Mark H. Carpenter [b]

[a] Department of Mathematics, North Carolina A&T State University, Greensboro, NC 27411, USA
[b] Computational Aerosciences Branch, NASA Langley Research Center, Hampton, VA 23681, USA

ARTICLE INFO

Article history:
Received 25 July 2008
Received in revised form 11 February 2009
Accepted 3 March 2009
Available online 12 March 2009

Keywords:
High-order finite difference methods
Weighted essentially non-oscillatory schemes
Energy estimate
Numerical stability
Artificial dissipation

ABSTRACT

A third-order Energy Stable Weighted Essentially Non-Oscillatory (ESWENO) finite difference scheme developed by the authors of this paper [N.K. Yamaleev, M.H. Carpenter, Third-order energy stable WENO scheme, J. Comput. Phys. 228 (2009) 3025–3047] was proven to be stable in the energy norm for both continuous and discontinuous solutions of systems of linear hyperbolic equations. Herein, a systematic approach is presented that enables "energy stable" modifications for existing WENO schemes of any order. The technique is demonstrated by developing a one-parameter family of fifth-order upwind-biased ESWENO schemes including one sixth-order central scheme; ESWENO schemes up to eighth order are presented in the Appendix. We also develop new weight functions and derive constraints on their parameters, which provide consistency, much faster convergence of the high-order ESWENO schemes to their underlying linear schemes for smooth solutions with arbitrary number of vanishing derivatives, and better resolution near strong discontinuities than the conventional counterparts.

1. Introduction

A new third-order weighted essentially non-oscillatory scheme (called *Energy Stable* WENO) has recently been proposed and developed by the authors of the present paper [1]. In [1], we prove that the third-order ESWENO scheme is energy stable, that is, stable in an L_2 energy norm, for systems of linear hyperbolic equations with both continuous and discontinuous solutions. Stability is explicitly achieved (by construction) by requiring that the ESWENO scheme satisfies a *nonlinear* summation-by-parts (SBP) condition at each instant in time. Thus, L_2 strict stability is attained without the need for a total variation bounded (TVB) flux reconstruction or a large-time-step constraint [2–5]. Herein, we generalize and extend the third-order ESWENO methodology [1] to an arbitrary order of accuracy. Similar to the third-order ESWENO scheme, the new families of higher order (up to eighth order) ESWENO schemes are provably stable in the energy norm and retain the underlying WENO characteristics of the background schemes. Numerical experiments demonstrate that the new family of ESWENO schemes provides the design order of accuracy for smooth problems and delivers stable essentially non-oscillatory solutions for problems with strong discontinuities.

Another issue that is addressed in this paper is the consistency of the new class of ESWENO schemes. The consistency of any WENO-type scheme fully depends on a proper choice of the weight functions. On one hand, for smooth solutions the weights should provide a rapid convergence of the WENO scheme to the corresponding underlying linear scheme. On the other hand, the weights should effectively bias the stencil away from strong discontinuities. The WENO reconstruction and weight functions that possess these properties were originally proposed by Liu et al. in [6] and later improved and

* Corresponding author. Tel.: +1 336 285 2093; fax: +1 336 256 0876.
E-mail address: nkyamale@ncat.edu (N.K. Yamaleev).

0021-9991/$ - see front matter © 2009 Elsevier Inc. All rights reserved.
doi:10.1016/j.jcp.2009.03.002

generalized by Jiang and Shu in [2]. It is well known that the high-order upwind-biased WENO schemes with conventional smoothness indicators developed in [2] are too dissipative for solving problems with a lot of structure in the smooth part of the solution, such as direct numerical simulation of turbulence or aeroacoustics [7,8]. Furthermore, as has been shown in [9,10], the classical weight functions of the fifth-order WENO scheme fail to provide the design order of convergence near smooth extrema, where the first derivative of the solution becomes equal to zero. Recently, new approaches are proposed in [9,10] to improve the error convergence near the critical points. Although these new weight functions recover the fifth order of convergence of the WENO scheme near smooth extrema, the problem persists if the first- and second-order derivatives vanish simultaneously [10]. An attempt to resolve this loss of accuracy is presented in [10]. This proposed resolution provides only a partial remedy for the problem; the same degeneration in the order of convergence occurs if at least the first three derivatives become equal to zero. To fully resolve this problem, we propose new weights to provide faster error convergence than those presented in [10], and impose some constraints on the weight parameters to guarantee that the WENO and ESWENO schemes are design-order accurate for sufficiently smooth solutions with an arbitrary number of vanishing derivatives.

This paper is organized as follows. In Section 2, energy estimates for the continuous and corresponding discrete wave equations are presented. In Section 3, we present a one-parameter family of fifth-order WENO schemes including one sixth-order central scheme. In Section 4, we present a systematic methodology for constructing ESWENO schemes of any order and demonstrate the methodology by transforming the family of WENO schemes presented in Section 3 into a family of fifth-order ESWENO schemes. In Section 5, we analyze the consistency of the new class of ESWENO schemes and derive sufficient conditions on the weight functions and formulae for evaluating their tuning parameters that ensure that the ESWENO schemes are design-order accurate regardless of the number of vanishing derivatives in the solution. In Section 6, we present numerical experiments that corroborate our theoretical results. We summarize and draw conclusions in Section 7.

2. Energy estimates

Consider a linear, scalar wave equation

$$\begin{aligned} &\frac{\partial u}{\partial t}+\frac{\partial f}{\partial x}=0, \quad f=au,\ t\geqslant 0,\ 0\leqslant x\leqslant 1,\\ &u(0,x)=u_0(x), \end{aligned} \tag{1}$$

where a is a constant, and $u_0(x)$ is a bounded piecewise continuous function. Without loss of generality, assume that $a \geqslant 0$, and further assume that the problem is periodic on the interval $0 \leqslant x \leqslant 1$. Applying the energy method to Eq. (1) leads to

$$\frac{d}{dt}\|u\|_{l_2}^2=0, \tag{2}$$

where $\|\cdot\|_{l_2}$ is the continuous l_2 norm. Thus, the continuous problem defined in Eq. (1) is neutrally stable.

Using mimetic techniques (see [1] or [11]), we now develop a class of discrete spatial operators that is neutrally stable or dissipative. The continuous target operator used for this development is the following singular perturbed wave equation:

$$\begin{aligned} &\frac{\partial u}{\partial t}+\frac{\partial f}{\partial x}=\sum_{n=1}^{N}(-1)^{n-1}\frac{\partial^n}{\partial x^n}\left(\mu_n\frac{\partial^n u}{\partial x^n}\right), \quad f=au,\ t\geqslant 0,\ 0\leqslant x\leqslant 1,\\ &u(0,x)=u_0(x), \end{aligned} \tag{3}$$

where $\mu_n=\mu_n(u), n=\overline{1,N}$ are nonnegative C^∞ functions of u. As before, we assume that Eq. (3) is subject to periodic boundary conditions. Our goal is to match each spatial term in Eq. (3) with an equivalent discrete term that maintains neutral stability (or dissipates) of the discrete energy norm.

We begin by showing that the terms on the right-hand side of Eq. (3) are dissipative thereby ensuring stability. Multiplying Eq. (3) by u and integrating it over the entire domain yields

$$\frac{1}{2}\frac{d}{dt}\|u\|_{l_2}^2+\frac{1}{2}au^2\Big|_0^1=\sum_{n=1}^{N}\int_0^1(-1)^{n-1}u\frac{\partial^n}{\partial x^n}\left(\mu_n\frac{\partial^n u}{\partial x^n}\right)dx. \tag{4}$$

Integrating each term on the right-hand side by parts and accounting for periodic boundary conditions yields the following energy estimate:

$$\frac{d}{dt}\|u\|_{l_2}^2=-2\sum_{n=1}^{N}\int_0^1\mu_n(u)\left(\frac{\partial^n u}{\partial x^n}\right)^2dx\leqslant 0. \tag{5}$$

All the perturbation terms included in Eq. (3) provide dissipation of energy.

Turning now to the discrete case, we define a uniform grid $x_j=j\Delta x, j=\overline{0,J}$, with $\Delta x=1/J$. On this grid, we define a flux $\bar{\mathbf{f}}=a\bar{\mathbf{u}}$ and its derivative $\bar{\mathbf{f}}_x=a\bar{\mathbf{u}}_x$, where $\bar{\mathbf{u}}=[u(x_0,t),\ldots,u(x_J,t)]^T$ and $\bar{\mathbf{u}}_x=[u_x(x_0,t),\ldots,u_x(x_J,t)]^T$ are projections of the continuous solution and its derivative onto the computational grid. Next, we define a pth-order approximation for the first-order derivative term in Eq. (1) as

$$\frac{\partial \bar{\mathbf{f}}}{\partial x} = D\bar{\mathbf{f}} + O(\Delta x^p). \tag{6}$$

Placing a mild restriction on the generality of the derivative operator (see [1] or [11]), the matrix D can be expressed in the following form:

$$\begin{aligned} &D = P^{-1}[Q + R]; \quad Q + Q^T = 0, \\ &R = R^T; \quad \mathbf{v}^T R\mathbf{v} \geqslant 0, \\ &P = P^T; \quad \mathbf{v}^T P\mathbf{v} > 0 \end{aligned} \tag{7}$$

for any real vector $\mathbf{v} \neq \mathbf{0}$. By choosing the matrix R as a discrete analog of the dissipation operator in Eq. (3), we have

$$R = \sum_{n=1}^{N} D_1^n \Lambda_n [D_1^n]^T, \tag{8}$$

where $\Lambda_n, n = \overline{1,N}$ are diagonal positive semidefinite matrices and D_1 is the difference matrix

$$D_1 = \begin{bmatrix} \ddots & \ddots & & 0 \\ & -1 & 1 & \\ 0 & & \ddots & \ddots \end{bmatrix}.$$

By using the SBP operators (6)–(8), Eq. (1) is discretized as follows:

$$\frac{\partial \mathbf{u}}{\partial t} + P^{-1}Q\mathbf{f} = -\sum_{n=1}^{N} P^{-1} D_1^n \Lambda_n [D_1^n]^T \mathbf{f}, \tag{9}$$

where $\mathbf{f} = a\mathbf{u}, \mathbf{u} = [u_0(t), u_1(t), \ldots, u_J(t),]^T$ is the discrete approximation of the solution u of Eq. (1), and Q and Λ_n are nonlinear matrices (i.e., $Q = Q(\mathbf{u})$ and $\Lambda_n = \Lambda_n(\mathbf{u})$). To show that the above finite difference scheme is stable, the energy method is used. Multiplying Eq. (9) with $\mathbf{u}^T P$ yields

$$\frac{1}{2}\frac{d}{dt}\|\mathbf{u}\|_P^2 + a\mathbf{u}^T Q\mathbf{u} = -a\sum_{n=1}^{N} \left([D_1^n]^T\mathbf{u}\right)^T \Lambda_n [D_1^n]^T \mathbf{u}, \tag{10}$$

where $\|\cdot\|_P$ is the P norm (i.e., $\|\mathbf{u}\|_P^2 = \mathbf{u}^T P\mathbf{u}$). Adding Eq. (10) to its transpose yields

$$\frac{d}{dt}\|\mathbf{u}\|_P^2 + a\mathbf{u}^T\left(Q + Q^T\right)\mathbf{u} = -2a\sum_{n=1}^{N} \left([D_1^n]^T\mathbf{u}\right)^T \Lambda_n [D_1^n]^T \mathbf{u}. \tag{11}$$

If we account for the periodic boundary conditions and the skew-symmetry of Q, then the second term on the left-hand side vanishes, and the energy estimate becomes

$$\frac{d}{dt}\|\mathbf{u}\|_P^2 = -2a\sum_{n=1}^{N} \left([D_1^n]^T\mathbf{u}\right)^T \Lambda_n [D_1^n]^T \mathbf{u} \leqslant 0. \tag{12}$$

The right-hand side of Eq. (12) is nonpositive because the diagonal matrices Λ_n, $n = \overline{1,N}$ are positive semidefinite (i.e., $\mathbf{v}^T\Lambda_n\mathbf{v} \geqslant 0$ for all real $\mathbf{v}$ of length $(J+1)$) and $a \geqslant 0$; thus the stability of the finite difference scheme given by Eq. (9) is assured. This result can be summarized in the following theorem.

Theorem 1. *The approximation (9) of the problem (1) is stable if* Eqs. (6)–(8) *hold.*

Remark 1. Despite the fact that the initial boundary value problem (1) is linear, the finite difference scheme (9) constructed for approximation of Eq. (1) is nonlinear, because the matrices Q and Λ_n (and in principle P) are assumed to depend on the discrete solution $\mathbf{u}$.

Remark 2. The only constraints that are imposed on the matrix Q and the diagonal matrices Λ_n are skew-symmetry of the former and positive semidefiniteness of the later. No other assumptions have been made about a specific form of the matrices Q and Λ_n to guarantee the stability of the finite difference scheme (9).

Remark 3. The discrete operators defined by Eqs. (6)–(8) are similar in form to those that are used for conventional SBP operators (see [11–13]). What is new, however, is the fact that the matrices Q and Λ_n depend on $\mathbf{u}$.

Remark 4. Note that high-order L_2-stable schemes given by Eq. (9) admit spurious oscillations near strong discontinuities or unresolved features. A systematic approach for constructing high-order WENO-type finite difference schemes of the form of Eq. (9) that provide both stability in the energy norm and good shock-capturing capabilities is presented in Section 4.

Remark 5. The proof of Theorem 1 does not directly extend to *nonlinear* hyperbolic equations with $f = a(u)u$. The principle difficulty in formulating a discrete energy estimate for the nonlinear case is the absence of a discrete "chain-rule" operator that mimics that of the continuous operator. Specifically, the diagonal matrix $A = A(\mathbf{u})$ representing $a(u)$ does not commute with the finite difference operators Q (or D_1), and thus the $QA + AQ^T$ does not vanish in the estimate. For the linear equation with $A = aI$, these commutative properties are used in Eqs. (10) and (11). Note that polynomial based methods (e.g., finite element methods) naturally satisfy the chain-rule property.

3. Fifth- and sixth-order WENO schemes

We now present a new one-parameter family of fifth-order WENO schemes and then use it as the starting point in the development of a family of "energy stable" WENO schemes. Any conventional high-order WENO finite difference scheme for the scalar one-dimensional wave equation (1) can be written in the following semidiscrete form:

$$\frac{du_j}{dt} + \frac{\hat{f}_{j+\frac{1}{2}} - \hat{f}_{j-\frac{1}{2}}}{\Delta x} = 0. \tag{13}$$

For the fifth-order WENO scheme that is presented in [2], the numerical flux $\hat{f}_{j+\frac{1}{2}}$ is computed as a convex combination of three third-order fluxes defined on the following three-point stencils: $S_{LL} = \{x_{j-2}, x_{j-1}, x_j\}, S_L = \{x_{j-1}, x_j, x_{j+1}\}$, and $S_R = \{x_j, x_{j+1}, x_{j+2}\}$ (see Fig. 1). Note that this set of stencils is not symmetric with respect to the $(j+\frac{1}{2})$ point; thus, the fifth-order WENO scheme is biased in the upwind direction. A central WENO scheme can be constructed form the conventional fifth-order WENO scheme by including an additional downwind candidate stencil $S_{RR} = \{x_{j+1}, x_{j+2}, x_{j+3}\}$, so that the collection of all four stencils is symmetric with respect to point $(j+\frac{1}{2})$. The WENO flux, constructed in this manner, is given by

$$\hat{f}_{j+\frac{1}{2}} = w^{LL}_{j+1/2} f^{LL}_{j+1/2} + w^{L}_{j+1/2} f^{L}_{j+1/2} + w^{R}_{j+1/2} f^{R}_{j+1/2} + w^{RR}_{j+1/2} f^{RR}_{j+1/2}, \tag{14}$$

where $f^{(r)}_{j+1/2}, r = \{LL, L, R, RR\}$ are third-order fluxes defined on these four stencils:

$$\begin{pmatrix} f^{LL}(u_{j+1/2}) \\ f^{L}(u_{j+1/2}) \\ f^{R}(u_{j+1/2}) \\ f^{RR}(u_{j+1/2}) \end{pmatrix} = \frac{1}{6} \begin{pmatrix} 2 & -7 & 11 & & & 0 \\ & -1 & 5 & 2 & & \\ & & 2 & 5 & -1 & \\ 0 & & & 11 & -7 & 2 \end{pmatrix} \begin{pmatrix} f(u_{j-2}) \\ f(u_{j-1}) \\ f(u_j) \\ f(u_{j+1}) \\ f(u_{j+2}) \\ f(u_{j+3}) \end{pmatrix} \tag{15}$$

and $w^{LL}, w^{L}, w^{R}, w^{RR}$ are weight functions that are assigned to four stencils S_{LL}, S_L, S_R, and S_{RR}, respectively. The above approach to constructing central WENO schemes is proposed in [8]. In general, high-order central WENO schemes that are built in this manner are unstable when unresolved features or strong discontinuities are present in the computational domain. In the next section, we present the generalized energy stable methodology to modify these WENO schemes to make them stable in the energy norm, while preserving their design order of accuracy and maintaining their non-oscillatory properties.

The terms w^{LL}, w^{L}, w^{R}, and w^{RR} in Eq. (14) are nonlinear weight functions. They have preferred values that are derived from an underlying linear scheme as well as solution dependent components. The preferred values are given by

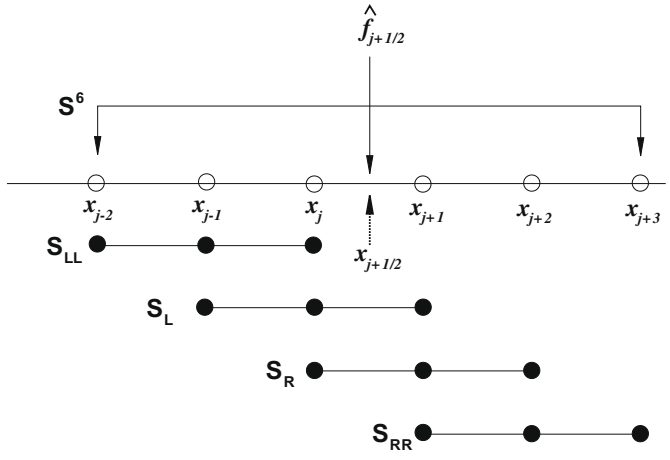

Fig. 1. The extended six-point stencil, S^6, and corresponding candidate stencils, S_{LL}, S_L, S_R, and S_{RR} for the one-parameter family of fifth-order WENO schemes.

$$d^{LL}=\frac{1}{10}-\varphi;\quad d^{L}=\frac{6}{10}-3\varphi;\quad d^{R}=\frac{3}{10}+3\varphi;\quad d^{RR}=\varphi, \tag{16}$$

where φ is a parameter. The convergence rate of the scheme (13)–(16) with the preferred values $w^{(r)}=d^{(r)}, r=\{LL,L,R,RR\}$ is equal to 5 for all values of the parameter φ in Eq. (16) except one specific value $\varphi_c=\frac{1}{20}$ for which the convergence rate is 6. In other words, the flux given by Eq. (14) defines a one-parameter family of fifth-order upwind-biased WENO schemes including one sixth-order central scheme corresponding to $\varphi_c=\frac{1}{20}$. The classical fifth-order upwind-biased WENO scheme of Jiang and Shu is obtained for $\varphi=0$.

We now present new weight functions that provide faster convergence of the WENO schemes to the corresponding underlying linear schemes for smooth solutions, and deliver improved shock-capturing capabilities near unresolved features. In Sections 5.2 and 5.3, we also derive some constraints on the weight function parameters to guarantee that the WENO and ESWENO schemes are design-order accurate for sufficiently smooth solutions with arbitrary number of vanishing derivatives. For the fifth- and sixth-order WENO schemes, these weights and smoothness indicators are given by

$$w_{j+\frac{1}{2}}^{(r)}=\frac{\alpha_r}{\sum_l \alpha_l}, \tag{17}$$

where

$$\alpha_r=d^{(r)}\left(1+\frac{\tau_p}{\epsilon+\beta_r}\right),\quad r=\{LL,L,R,RR\} \tag{18}$$

and ϵ is a small positive parameter that can depend on Δx. The functions $\beta^{(r)}$ are the classical smoothness indicators (see Eq. (59) for the general expression). For fifth-order schemes, they are given by

$$\begin{aligned}
\beta^{LL}&=\frac{13}{12}\left(f_{j-2}-2f_{j-1}+f_j\right)^2+\frac{1}{4}\left(f_{j-2}-4f_{j-1}+3f_j\right)^2,\\
\beta^{L}&=\frac{13}{12}\left(f_{j-1}-2f_j+f_{j+1}\right)^2+\frac{1}{4}\left(f_{j-1}-f_{j+1}\right)^2,\\
\beta^{R}&=\frac{13}{12}\left(f_j-2f_{j+1}+f_{j+2}\right)^2+\frac{1}{4}\left(3f_j-4f_{j+1}+f_{j+2}\right)^2,\\
\beta^{RR}&=\frac{13}{12}\left(f_{j+1}-2f_{j+2}+f_{j+3}\right)^2+\frac{1}{4}\left(-5f_{j+1}+8f_{j+2}-3f_{j+3}\right)^2.
\end{aligned} \tag{19}$$

The expression for τ_5 is given by

$$\tau_5=\begin{cases}\left(-f_{j-2}+5f_{j-1}-10f_j+10f_{j+1}-5f_{j+2}+f_{j+3}\right)^2, & \text{for } \varphi\neq 0,\\ \left(f_{j-2}-4f_{j-1}+6f_j-4f_{j+1}+f_{j+2}\right)^2, & \text{for } \varphi=0,\end{cases} \tag{20}$$

which represents a quadratic function of the fifth-degree undivided difference defined on the entire six-point stencil and provides the highest order information that is possible on this stencil. Note that for the conventional fifth-order WENO scheme that corresponds to $\varphi=0$, the downwind stencil S_{RR} is not available; therefore, only the fourth-degree undivided difference can be built on this five-point stencil. Expressions for the fourth-, seventh-, and eighth-order WENO schemes are given in the Appendix.

The new weight functions given by Eqs. (17)–(20) differ from those used in the original algorithm by Jiang and Shu [2]. For example, Eq. (18) replaces the expression

$$\alpha_r=\frac{d^{(r)}}{\left(\epsilon+\beta^{(r)}\right)^2} \tag{21}$$

that is used in [2]. Eqs. (17)–(20) more closely resemble the weight functions proposed by Borges et al. in [10]. There are differences, however, in how the function τ_p and the parameters ϵ are chosen. In [10], the following function $\tilde{\tau}_5$ is proposed:

$$\tilde{\tau}_5=|\beta_{LL}-\beta_R|. \tag{22}$$

Although the weight functions (17)–(19) with $\tilde{\tau}_5$ given by Eq. (22) significantly outperform the conventional weights of Jiang and Shu for both continuous and discontinuous solutions, three remaining shortcomings include:

(1) The function $\tilde{\tau}_5$ given by Eq. (22) is not smooth, because an absolute value function is used, which may cause a loss of accuracy at points where $\beta_{LL}-\beta_R$ changes sign.
(2) This approach does not generalize to WENO schemes with design orders other than 5. For example, neither $\tilde{\tau}_6=|\beta_{LL}-\beta_R|$ nor $\tilde{\tau}_6=|\beta_{LL}-\beta_{RR}|$ provides the design order of accuracy for the sixth-order central WENO scheme.

(3) Near critical points where f', f'' and f''' vanish simultaneously, the modified weights (17)–(19), (22) fail to provide the design order of convergence for the fifth-order WENO scheme, if no constraints are imposed on the parameter ϵ other than $\epsilon > 0$. An example that demonstrates this property is presented in Section 6.1.

The new function τ_5 defined by Eq. (20) circumvents the first and second drawbacks encountered when using $\tilde{\tau}_5$ suggested in [10]. Indeed, τ_5 is a C^∞ function in its arguments. Equation (20) can readily be generalized to WENO schemes of order p by choosing τ_p to be the pth-degree undivided difference defined on the entire $(p+1)$-point stencil. In contrast to $\tilde{\tau}_5$, which is $O(\Delta x^5)$ for smooth solutions, the proposed function τ_5 given by Eq. (20) is of order $O(\Delta x^8)$ and $O(\Delta x^{10})$ for $\varphi = 0$ and $\varphi \neq 0$, respectively; thus much faster convergence of the fifth- and sixth-order WENO schemes to the corresponding underlying linear schemes is achieved.

A remedy for the third shortcoming requires an additional modification to the approach proposed in [10]. Both the fifth- and sixth-order WENO schemes with the new weights given by Eqs. (17)–(20) are design-order accurate for smooth solutions, including points at which the first and second-order derivatives of the solution vanish simultaneously. However, if all derivatives up to the third order are equal to zero and no constraint is imposed on the parameter ϵ, then the fifth- and sixth-order WENO schemes locally become only third-order accurate. An example illustrating this degeneration in accuracy is presented in Section 6.1. To fully resolve this issue, some constraints should be imposed on the parameter ϵ. This issue is addressed in Section 5.3.

4. A general approach to constructing high-order energy stable schemes

A systematic approach is needed to extend the "energy stable" modifications developed for the third-order WENO scheme [1] to existing higher order, one-dimensional finite difference WENO schemes. The following algorithm transforms an existing WENO scheme into an ESWENO scheme that is characterized by the following four properties: (1) a bounded energy estimate for arbitrary nonsmooth initial data, (2) conservation, (3) the design order of accuracy for sufficiently smooth data, and (4) discontinuity (shock) capturing capabilities that are similar to those of the base WENO scheme.

Algorithm 1. (Transformation from WENO to ESWENO)

(1) Express the base WENO derivative operator as matrix D.
(2) Decompose D into symmetric and skew-symmetric components as

$$D = D_{skew} + D_{sym}.$$

(3) Add an artificial dissipation operator $\overline{D}_{ad}$ such that the modified symmetric matrix $D_{sym} + \overline{D}_{ad}$ is positive semidefinite.
   (a) Form the decomposition $D_{sym} = \sum_{i=0}^{s} [D_1^i] \Lambda_i [D_1^i]^T$, where $2s+1$ is the bandwidth of the matrix D. The existence of this decomposition is established in the Appendix.
   (b) Modify the diagonal terms of Λ_i such that they are smoothly positive. One such approach is

$$(\bar{\lambda}_i)_{j,j} = \frac{1}{2}\left[\sqrt{(\lambda_i)_{j,j}^2 + \delta_i^2} - (\lambda_i)_{j,j}\right], \tag{23}$$

where $\delta_i, 0 \leqslant i \leqslant s$ are small positive constants that may depend on Δx.
   (c) Form the symmetric, positive semidefinite matrix

$$\overline{D}_{ad} = P^{-1} \sum_{i=0}^{s} [D_1^i] \bar{\Lambda}_i [D_1^i]^T. \tag{24}$$

(4) Form the energy stable operator

$$\overline{D} = D + \overline{D}_{ad}. \tag{25}$$

By construction, Algorithm 1 is applicable to 1-D periodic schemes of any order and produces a modified scheme that automatically satisfies the first and second properties: bounded energy estimate and conservation (see [1] for details). Likewise, as shown in the next section, the additional terms added in the ESWENO formulation do not degrade the formal accuracy of the original WENO discretization (property three). However, the degree to which the two formulations differ for unresolved data is not clear. Thus, this property of the new ESWENO scheme must be tested to ensure it retains good shock-capturing capabilities of the original formulation.

4.1. Fifth- and sixth-order ESWENO schemes

We now apply Algorithm 1 to the one-parameter family of fifth-order WENO schemes Eqs. (17)–(20) for the scalar 1-D wave Eq. (1) with $a \geqslant 0$. Combining Eq. (15) with Eq. (14) and substituting the resulting WENO flux $\hat{f}_{j+\frac{1}{2}}$ into Eq. (13) produces a stencil for the jth grid point of the form

$$D^5_{j,:} = \frac{1}{6\Delta x}\left(\begin{array}{c|c|c|c|c|c|c} 0 & 2w^{LL}_{j+1/2} & -7w^{LL}_{j+1/2} & 11w^{LL}_{j+1/2} & 0 & 0 & 0 \\ 0 & 0 & -1w^{L}_{j+1/2} & 5w^{L}_{j+1/2} & 2w^{L}_{j+1/2} & 0 & 0 \\ 0 & 0 & 0 & 2w^{R}_{j+1/2} & 5w^{R}_{j+1/2} & -1w^{R}_{j+1/2} & 0 \\ 0 & 0 & 0 & 0 & 11w^{RR}_{j+1/2} & -7w^{RR}_{j+1/2} & 2w^{RR}_{j+1/2} \\ -2w^{LL}_{j-1/2} & 7w^{LL}_{j-1/2} & -11w^{LL}_{j-1/2} & 0 & 0 & 0 & 0 \\ 0 & 1w^{L}_{j-1/2} & -5w^{L}_{j-1/2} & -2w^{L}_{j-1/2} & 0 & 0 & 0 \\ 0 & 0 & -2w^{R}_{j-1/2} & -5w^{R}_{j-1/2} & 1w^{R}_{j-1/2} & 0 & 0 \\ 0 & 0 & 0 & -11w^{RR}_{j-1/2} & 7w^{RR}_{j-1/2} & -2w^{RR}_{j-1/2} & 0 \end{array}\right)\begin{pmatrix} f(u_{j-3}) \\ f(u_{j-2}) \\ f(u_{j-1}) \\ f(u_j) \\ f(u_{j+1}) \\ f(u_{j+2}) \\ f(u_{j+3}) \end{pmatrix} \tag{26}$$

An explicit expression for the differentiation matrix D^5 follows immediately from Eq. (26).

The derivative matrix D^5 is now decomposed into symmetric and skew-symmetric parts as

$$D^5 = D^5_{skew} + D^5_{sym}.$$

As with the third-order case [1], the skew-symmetric component of D^5 and the norm take the form

$$D^5_{skew} = P^{-1}Q_5; \quad Q_5 + Q_5^T = 0; \quad P = \Delta x I,$$

while the matrix D^5_{sym} is expressed as

$$D^5_{sym} = P^{-1}\left(D^3_1\Lambda^5_3[D^3_1]^T + D^2_1\Lambda^5_2[D^2_1]^T + D^1_1\Lambda^5_1[D^1_1]^T + D^0_1\Lambda^5_0[D^0_1]^T\right). \tag{27}$$

The matrices $\Lambda^5_k, k = \overline{0,3}$ are diagonal with expressions for the jth element defined by

$$(\lambda^5_3)_{jj} = \frac{1}{6}\left[w^{LL}_{j+5/2} - w^{RR}_{j+1/2}\right], \tag{28}$$

$$(\lambda^5_2)_{jj} = \frac{1}{12}\left[w^{LL}_{j+3/2} - 4w^{LL}_{j+5/2} + w^{L}_{j+3/2} - w^{R}_{j+1/2} + 4w^{RR}_{j-1/2} - w^{RR}_{j+1/2}\right], \tag{29}$$

$$(\lambda^5_1)_{jj} = \frac{1}{12}\left[3w^{LL}_{j+1/2} - 5w^{LL}_{j+3/2} + 2w^{LL}_{j+5/2} + w^{L}_{j+1/2} - w^{L}_{j+3/2} + w^{R}_{j-1/2} - w^{R}_{j+1/2} - 2w^{RR}_{j-3/2} + 5w^{RR}_{j-1/2} - 3w^{RR}_{j+1/2}\right], \tag{30}$$

$$(\lambda^5_0)_{jj} = \frac{1}{2}\left[-w^{LL}_{j-1/2} - w^{L}_{j-1/2} - w^{R}_{j-1/2} - w^{RR}_{j-1/2} + w^{LL}_{j+1/2} + w^{L}_{j+1/2} + w^{R}_{j+1/2} + w^{RR}_{j+1/2}\right] = 0. \tag{31}$$

Because $\sum_r w^{(r)}_{:} = 1$, Λ^5_0 is always equal to zero, and is not included in $\overline{D}^5_{ad}$. The diagonal terms $(\lambda^5_i)_{jj}, i = 1,2,3$ could be either positive or negative; thus, the conventional fifth- and sixth-order WENO schemes may become locally unstable. Defining $(\bar{\lambda}^5_i)_{jj}, i = 1,2,3$ to be smoothly positive

$$(\bar{\lambda}^5_i)_{jj} = \frac{1}{2}\left[\sqrt{(\lambda^5_i)^2_{jj} + \delta^2_i} - (\lambda^5_i)_{jj}\right],$$

the additional artificial dissipation operator becomes $\overline{D}^5_{ad} = P^{-1}\sum_{i=1}^3 [D^i_1](\bar{\Lambda}^5_i)[D^i_1]^T$, and the resulting energy stable scheme is obtained by adding the additional dissipation term to the original WENO scheme. That is,

$$\overline{D}^5 = D^5 + \overline{D}^5_{ad}. \tag{32}$$

By construction, $\overline{D}^5$ satisfies all of the conditions of Theorem 1, thereby providing stability of the fifth- and sixth-order ESWENO schemes that are defined by Eq. (32).

5. Consistency analysis

5.1. Necessary and sufficient conditions for consistency of WENO schemes

We now derive necessary and sufficient conditions for the weight functions $w^{(r)}_{:}$ for a family of pth-order WENO schemes to attain the design order of accuracy. Similar conditions have been obtained for the conventional fifth-order WENO scheme in [9]. With the same approach discussed in Section 3 for $p = 5$, a one-parameter family of pth-order WENO fluxes can be constructed by using a convex combination of $(s+1)$ fluxes $f^{(r)}_{:}$ of sth order as

$$\hat{f}_{j\pm1/2} = \sum_r w^{(r)}_{j\pm1/2} f^{(r)}_{j\pm1/2}, \tag{33}$$

with

$$f^{(r)}_{j\pm1/2} = h(x_{j\pm1/2}) + \sum_{l=s}^{p} c^{(r)}_l \Delta x^l + O(\Delta x^{p+1}), \tag{34}$$

where $h(x)$ is the numerical flux function that is implicitly defined as

$$f(x) = \frac{1}{\Delta x}\int_{x-\frac{\Delta x}{2}}^{x+\frac{\Delta x}{2}} h(\eta)d\eta \tag{35}$$

and $c_l^{(r)}$ are constants that do not depend on Δx.

The corresponding pth-order WENO operator that approximates the first-order spatial derivative is given by

$$[D^p\mathbf{f}]_j = \frac{\hat{f}_{j+1/2} - \hat{f}_{j-1/2}}{\Delta x} = \frac{\sum_r \left(w_{j+1/2}^{(r)} f_{j+1/2}^{(r)} - w_{j-1/2}^{(r)} f_{j-1/2}^{(r)}\right)}{\Delta x}, \tag{36}$$

where $[\cdot]_j$ is a jth component of a vector, the index r in Eq. (36) sweeps over all $(s+1)$ stencils, and $w^{(r)}$ is a nonlinear weight function that is assigned to the corresponding s-point stencil S_r. For sufficiently smooth solutions, the weights $w_i^{(r)}$ approach their preferred values $d^{(r)}$, so that the WENO operator converges to the following target linear operator D^{Target}:

$$\left[D^{\text{Target}}\mathbf{f}\right]_j = \frac{f_{j+1/2}^{\text{Target}} - f_{j-1/2}^{\text{Target}}}{\Delta x} = \frac{\sum_r \left(d^{(r)} f_{j+1/2}^{(r)} - d^{(r)} f_{j-1/2}^{(r)}\right)}{\Delta x}, \tag{37}$$

where $d^{(r)}$ is a one-parameter family of constants chosen to ensure pth-order convergence of the target operator to the exact value of the first-order derivative at x_j. That is,

$$\left[D^{\text{Target}}\mathbf{f}\right]_j = \left.\frac{\partial f}{\partial x}\right|_{x=x_j} + O(\Delta x^p). \tag{38}$$

The coefficients $d^{(r)}$ for one-parameter families of linear target schemes up to eighth order are given in the Appendix. All target linear schemes in the family are $(2s-1)$th-order accurate, except one central scheme, which is $(2s)$th-order accurate.

Subtracting Eq. (37) from Eq. (36) and using Eq. (34), we have

$$\begin{aligned}
[D^p\mathbf{f}]_j - \left[D^{\text{Target}}\mathbf{f}\right]_j &= \frac{\sum_r \left[(w_{j+1/2}^{(r)} - d^{(r)}) f_{j+1/2}^{(r)} - (w_{j-1/2}^{(r)} - d^{(r)}) f_{j-1/2}^{(r)}\right]}{\Delta x} \\
&= \frac{1}{\Delta x}\sum_r \left[(w_{j+1/2}^{(r)} - d^{(r)}) h(x_{j+1/2}) - (w_{j-1/2}^{(r)} - d^{(r)}) h(x_{j-1/2})\right] \\
&\quad + \sum_{l=s}^{p}\sum_r \Delta x^{l-1} c_l^{(r)}\left[(w_{j+1/2}^{(r)} - d^{(r)}) - (w_{j-1/2}^{(r)} - d^{(r)})\right] + O(\Delta x^p).
\end{aligned} \tag{39}$$

From Eq. (39) it immediately follows that to retain pth-order accuracy, the weights of the WENO operator D^p should satisfy the following necessary and sufficient conditions:

$$\begin{aligned}
&\sum_r \left[w_{j\pm1/2}^{(r)} - d^{(r)}\right] = O(\Delta x^{p+1}), \\
&\sum_r c_s^{(r)}\left[(w_{j+1/2}^{(r)} - d^{(r)}) - (w_{j-1/2}^{(r)} - d^{(r)})\right] = O(\Delta x^{p-s+1}), \\
&\cdots \\
&\sum_r c_p^{(r)}\left[(w_{j+1/2}^{(r)} - d^{(r)}) - (w_{j-1/2}^{(r)} - d^{(r)})\right] = O(\Delta x).
\end{aligned} \tag{40}$$

Here, we use the following properties of $h(x)$ and $d^{(r)}$: $f'(x) = \frac{h(x_{j+1/2}) - h(x_{j-1/2})}{\Delta x}$, and $\sum_r d^{(r)} = 1$.

By construction, the weights (17) are normalized such that $\sum_r w_i^{(r)} = 1$; thus, the first constraint in Eq. (40) is satisfied identically. To simplify the analysis, especially for $f(x)$ with an arbitrary number of vanishing derivatives, we hereafter use the following sufficient condition on $w_i^{(r)}$ for the family of WENO schemes to attain pth-order accuracy:

$$w_i^{(r)} - d^{(r)} = O(\Delta x^{p-s+1}). \tag{41}$$

This constraint is a direct consequence of the necessary and sufficient conditions (40).

5.2. Sufficient conditions for consistency of ESWENO schemes

In this section, we show that the conditions (41) and the following constraints on δ_i in Eq. (23):

$$\delta_i = O(\Delta x^{p-2i+1}), \quad 1 \leqslant i \leqslant s \tag{42}$$

guarantee that the energy stable modifications of the conventional pth-order WENO scheme (see Section 4) preserve the design order of the original scheme. As follows from Eq. (25), the ESWENO operator consists of two terms: one is the original WENO operator and the other is the additional artificial dissipation operator $\overline{D}_{ad}$ given by Eq. (24). As shown in the previous section, the WENO operator is pth-order accurate if Eq. (41) holds. Hence, we need only show that $\overline{D}_{ad}\mathbf{f} = O(\Delta x^p)$.

Let us prove this conjecture for the one-parameter family of fifth-order ESWENO schemes presented in Section 4.1. Note that the term $P^{-1}D_1^3\Lambda_0[D_1^3]^T$ in Eq. (27) is identically equal to zero because of the normalization $\sum_r w_{:}^{(r)} = 1$ and is, therefore, not included in $\overline{D}_{ad}$. Thus, the additional artificial dissipation term is given by

$$\overline{D}_{ad}\mathbf{f} = P^{-1}D_1\bar{\Lambda}_1[D_1]^T\mathbf{f} + P^{-1}D_1^2\bar{\Lambda}_2[D_1^2]^T\mathbf{f} + P^{-1}D_1^3\bar{\Lambda}_3[D_1^3]^T\mathbf{f}, \tag{43}$$

$$\bar{\lambda}_i = \frac{1}{2}\left[\sqrt{\lambda_i^2+\delta_i^2} - \lambda_i\right], \quad i = 1,2,3, \tag{44}$$

where $\bar{\lambda}_i$ is a jth diagonal element of the matrix $\bar{\Lambda}_i$. For simplicity, we have omitted the superscript 5 and the subscript (j,j) in this section.

First, we evaluate the terms λ_1, λ_2, and λ_3 that are defined by Eqs. (28)–(30). To simplify the derivation, the sufficient conditions (41) for the one-parameter family of fifth-order ESWENO schemes is rewritten in the following form:

$$w_{:}^{(r)} - d^{(r)} = \left(\varphi - \frac{1}{20}\right)O(\Delta x^3) + O(\Delta x^4). \tag{45}$$

In Eq. (45), it has been taken into account that the stencil width s of each reconstruction polynomial is equal to 3, and the order p of this family of schemes is equal to 5 if $\varphi \neq \frac{1}{20}$ or 6 if $\varphi = \frac{1}{20}$. As follows from Eq. (45), the stiffer constraint on the weights should be imposed to obtain sixth-order accuracy.

Replacing $w_{:}^{(r)}$ in λ_2 with the corresponding preferred values $d^{(r)}$ and using Eqs. (16) and (29), for any value of the parameter φ, we have

$$\frac{1}{12}\left[d^{LL} - 4d^{L} + d^{L} - d^{R} + 4d^{RR} - d^{RR}\right] \equiv 0. \tag{46}$$

Subtracting Eq. (46) from Eq. (29) and taking into account Eq. (45) yields

$$\begin{aligned}\lambda_2 &= \frac{1}{12}\left[(w_{j+3/2}^{LL} - d^{LL}) - 4(w_{j+5/2}^{LL} - d^{LL}) + (w_{j+3/2}^{L} - d^{L}) - (w_{j+1/2}^{R} - d^{R}) + 4(w_{j-1/2}^{RR} - d^{RR}) - (w_{j+1/2}^{RR} - d^{RR})\right] \\ &= \left(\varphi - \frac{1}{20}\right)O(\Delta x^3) + O(\Delta x^4).\end{aligned} \tag{47}$$

By comparing Eqs. (29) and (30), one can see that the order of λ_1 is at least one higher than that of λ_2 because of the additional cancellation that occurs within each group of terms associated with the same stencil. For example, expanding all of the terms $w_{:}^{LL}$ in Eq. (30) about x_j yields

$$3w_{j+1/2}^{LL} - 5w_{j+3/2}^{LL} + 2w_{j+5/2}^{LL} = -2\left.\frac{\partial w^{LL}}{\partial x}\right|_{x_j}\Delta x + O(\Delta x^2), \tag{48}$$

which gives an extra factor $O(\Delta x)$ compared with the corresponding terms $w_{:}^{LL}$ in Eq. (30): $w_{j+3/2}^{LL} - 4w_{j+5/2}^{LL} = O(1)$. The same conclusion can be drawn for the other groups of terms that are associated with the L, R, and RR stencils in Eq. (30), which leads to

$$\lambda_1 = \left(\varphi - \frac{1}{20}\right)O(\Delta x^4) + O(\Delta x^5). \tag{49}$$

Applying the same procedure to λ_3 yields

$$\lambda_3 = \frac{1}{6}\left(d^{LL} - d^{RR}\right) + \frac{1}{6}\left[(w_{j+5/2}^{LL} - d^{LL}) - (w_{j+1/2}^{RR} - d^{RR})\right] = \frac{1}{6}\left(\frac{1}{10} - 2\varphi\right) + \left(\varphi - \frac{1}{20}\right)O(\Delta x^3) + O(\Delta x^4). \tag{50}$$

To evaluate each term in Eq. (43), we consider three cases: (1) $|\lambda_i| \gg \delta_i > 0$, (2) $\lambda_i = O(\delta_i)$, and (3) $|\lambda_i| \ll \delta_i, i = 1,2,3$. If we assume that $|\lambda_i| \gg \delta_i > 0$, then Eq. (44) can be expanded as follows:

$$\bar{\lambda}_i = \frac{|\lambda_i| - \lambda_i}{2} + \frac{\delta_i^2}{4|\lambda_i|}, \tag{51}$$

which yields

$$\bar{\lambda}_i = \begin{cases} |\lambda_i|, & \text{if } \lambda_i < 0, \\ \delta_i, & \text{if } \lambda_i = 0, \\ \frac{\delta_i^2}{4|\lambda_i|}, & \text{if } \lambda_i > 0, \end{cases} \tag{52}$$

where the higher order terms have been omitted. Because Eq. (52) has been derived under the assumption that $|\lambda_i| \gg \delta_i > 0$, we can immediately conclude that $|\lambda_i| \gg \delta_i \gg \frac{\delta_i^2}{4|\lambda_i|}$. Therefore, we only need consider that

$$\bar{\lambda}_i = |\lambda_i|, \tag{53}$$

which provides the lowest order of convergence for the term $D_i^i \bar{A}_i [D_1^i]^T \mathbf{f}$. Substituting Eq. (53) in Eq. (43) and using Eqs. (47), (49), (50), the additional ESWENO dissipation term becomes

$$\overline{D}_{ad}\mathbf{f} = \left[\left(\varphi - \frac{1}{20}\right)O(\Delta x^3) + O(\Delta x^4)\right] D_1 [D_1]^T \mathbf{f} + \left[\left(\varphi - \frac{1}{20}\right)O(\Delta x^2) + O(\Delta x^3)\right] D_1^2 [D_1^2]^T \mathbf{f} + \left[\frac{\frac{1}{10} - 2\varphi}{6\Delta x} + \left(\varphi - \frac{1}{20}\right)O(\Delta x^2) + O(\Delta x^3)\right] D_1^3 [D_1^3]^T \mathbf{f}. \tag{54}$$

Taking into account that $D_1^i [D_1^i]^T \mathbf{f} = O(\Delta x^{2i}), \overline{D}_{ad}\mathbf{f}$ can be recast as

$$\overline{D}_{ad}\mathbf{f} = \left(\varphi - \frac{1}{20}\right)O(\Delta x^5) + O(\Delta x^6). \tag{55}$$

Form Eq. (55) it follows that the additional dissipation term is fifth-order accurate for all values of the parameter φ except $\varphi = \frac{1}{20}$; for this value, the order increases from 5 to 6.

The second case can be considered in a similar manner. Substituting $\lambda_i = O(\delta_i), i = 1, 2, 3$ in Eq. (43) yields

$$\overline{D}_{ad}\mathbf{f} = \frac{O(\delta_1)}{\Delta x} D_1 [D_1]^T \mathbf{f} + \frac{O(\delta_2)}{\Delta x} D_1^2 [D_1^2]^T \mathbf{f} + \frac{O(\delta_3)}{\Delta x} D_1^3 [D_1^3]^T \mathbf{f} = O(\delta_1 \Delta x) + O(\delta_2 \Delta x^3) + O(\delta_3 \Delta x^5). \tag{56}$$

To guarantee that the ESWENO dissipation term is pth-order accurate, the following constraints should be imposed on δ_i:

$$\begin{aligned} \delta_1 &= O(\Delta x^{p-1}), \\ \delta_2 &= O(\Delta x^{p-3}), \\ \delta_3 &= O(\Delta x^{p-5}), \end{aligned} \tag{57}$$

where p is equal to 5 for $\varphi \neq \frac{1}{20}$ or 6 for $\varphi = \frac{1}{20}$. Note that the constraints (57) are fully consistent with those given by Eq. (42). The third case, $|\lambda_i| \ll \delta_i$, is very similar to the second one and results in the same constraints (57) on δ_i; therefore, the third case is not presented here.

Remark 6. Note that $\delta_i, i = 1, 2, 3$ are user-defined parameters; therefore, the conditions (42) can always be met.

Remark 7. Although only fifth- and sixth-order ESWENO schemes have been analyzed in this section, the same procedure is directly applicable to the other ESWENO schemes presented in the Appendix. Thus, we can conclude that if Eqs. (41) and (42) hold, then all the ESWENO schemes considered in this paper are design-order accurate.

5.3. Consistency of the ESWENO scheme with new weights

The new weight functions for the one-parameter family of pth-order WENO and ESWENO schemes are given by

$$w^{(r)} = \frac{\alpha_r}{\sum_l \alpha_l}, \quad \alpha_r = d_r \left(1 + \frac{\tau_p}{\epsilon + \beta^{(r)}}\right), \tag{58}$$

where $\beta^{(r)}$ are the classical smoothness indicators:

$$\beta^{(r)} = \sum_{l=1}^{s-1} \Delta x^{2l-1} \int_{x_{j-\frac{1}{2}}}^{x_{j+\frac{1}{2}}} \left(\frac{d^l q_r(x)}{d^l x}\right)^2 dx, \tag{59}$$

$q_r(x)$ is an $(s-1)$th-degree reconstruction polynomial defined on a stencil S_r, and ϵ is a small positive parameter that can depend on Δx. In Eq. (58), τ_p is defined by

$$\tau_p = \left(V\langle x_{j-s+1}, \ldots, x_{j+s}\rangle\right)^2, \quad \text{for } \varphi \neq 0, \tag{60}$$

$$\tau_p = \left(V\langle x_{j-s+1}, \ldots, x_{j+s-1}\rangle\right)^2, \quad \text{for } \varphi = 0, \tag{61}$$

where $V\langle x_{j-s+1}, \ldots, x_{j+s}\rangle$ is the pth-degree undivided difference. Note that for the original WENO schemes of Jiang and Shu [2], which correspond to $\varphi = 0$, the entire stencil includes only $(2s-1)$ points; therefore, the highest degree of undivided differences that can be constructed on this stencil is $2s-2$, rather than $2s-1$ as for the other schemes in this one-parameter family. In particular, $w^{(r)}, \beta^{(r)}$, and τ_5 for the fifth- and sixth-order WENO and ESWENO schemes are given by Eqs. (17)–(20). Another scheme that requires special consideration is the central ESWENO scheme, which is obtained by setting $\varphi = \varphi_c$, so that its order is one higher than that of the other schemes in the family.

First, we present a truncation error analysis for the entire one-parameter family of pth-order ESWENO schemes, except for the two schemes that correspond to $\varphi = 0$ and $\varphi = \varphi_c$. We show that the new weights defined by Eqs. (58)–(60) satisfy the sufficient condition (41) for smooth solutions with any number of vanishing derivatives if the following constraint is imposed on the parameter ϵ in Eq. (58):

$$\epsilon \geqslant O(\Delta x^{p+s-1}) > 0, \tag{62}$$

where p is a design order of the scheme and $(s-1)$ is a degree of the corresponding reconstruction polynomials.

Assuming that all of the required derivatives are continuous and using the properties of the Newton undivided differences, Taylor series expansions of $\beta^{(r)}$ and τ_p ($\varphi \neq 0$) at x_j are given by

$$\beta^{(r)} = f'^2 \Delta x^2 + O(\Delta x^3), \tag{63}$$

$$\tau_p = (f^{(p)})^2 \Delta x^{2p} + O(\Delta x^{2p+1}), \tag{64}$$

where f' and $f^{(p)}$ are the first- and pth-order derivatives of f at x_j. For example, for the family of the fifth-order WENO schemes, these expansions are

$$\begin{aligned}
\beta^{LL} &= f'^2 \Delta x^2 + \left(\frac{13}{12} f''^2 - \frac{2}{3} f' f'''\right)\Delta x^4 + \left(-\frac{13}{6} f'' f''' + \frac{1}{2} f' f''''\right)\Delta x^5 + O(\Delta x^6),\\
\beta^{L} &= f'^2 \Delta x^2 + \left(\frac{13}{12} f''^2 + \frac{1}{3} f' f'''\right)\Delta x^4 + O(\Delta x^6),\\
\beta^{R} &= f'^2 \Delta x^2 + \left(\frac{13}{12} f''^2 - \frac{2}{3} f' f'''\right)\Delta x^4 + \left(\frac{13}{6} f'' f''' - \frac{1}{2} f' f''''\right)\Delta x^5 + O(\Delta x^6),\\
\beta^{RR} &= f'^2 \Delta x^2 + \left(\frac{13}{12} f''^2 - \frac{11}{3} f' f'''\right)\Delta x^4 + \left(\frac{13}{3} f'' f''' - 5 f' f''''\right)\Delta x^5 + O(\Delta x^6),
\end{aligned} \tag{65}$$

$$\tau_5 = \left(f^{(5)}\right)^2 \Delta x^{10} + O(\Delta x^{11}), \quad \text{for } \varphi \neq 0. \tag{66}$$

We first consider a case with $f'(x_j) \neq 0$. Substituting Eqs. (63) and (64) in Eq. (58) and accounting for Eq. (62) yields

$$\frac{\tau_p}{\epsilon + \beta_r} = O(\Delta x^{2p-2})\left(1 - O(\Delta x^{p+s-3})\right), \tag{67}$$

which leads to

$$w^{(r)} = d^{(r)} + O(\Delta x^{2p-1}). \tag{68}$$

Note that the order of convergence of $w^{(r)}$ to its preferred value is $2p-1$ rather than $2p-2$. The main reason for such "superconvergence" is the additional cancellation that occurs because the leading truncation error terms of all of the smoothness indicators are identical to each other if $f' \neq 0$, as can be seen in Eq. (63). Eqs. (67) and (68) are valid only for $p \geqslant 3$ and are not applicable to the third-order WENO and ESWENO schemes that correspond to $\varphi = 0$. The detailed analysis of these third-order schemes ($\varphi = 0$) is presented in [1], which is beyond the scope of this paper. By comparing Eq. (68) with Eq. (41), we can immediately conclude that the new weights satisfy the sufficient condition (41), ensuring that both the WENO and ESWENO schemes are design-order accurate. Furthermore, for schemes of order 3 ($\varphi \neq 0$) or higher, the weights converge to their preferred values at a rate that is significantly faster than that given by the sufficient condition (41). The result is a much faster convergence for both the ESWENO and WENO schemes to the corresponding target linear schemes even on coarse and moderate grids.

The next issue that is addressed is the convergence of the ESWENO schemes near the critical points at which the first-order and higher order derivatives of the flux approach zero. Let x_c be a critical point at which the flux function is sufficiently smooth and its derivatives up to n_{vd}th order are equal to zero, i.e.,

$$f'(x_c) = \cdots = f^{(n_{vd})}(x_c) = 0, \quad f^{(n_{vd}+1)}(x_c) \neq 0.$$

In contrast to the previous case for which $f' \neq 0$, the leading truncation error terms of the smoothness indicators at the critical point are not equal to each other; thus, no additional cancellation occurs. For any number of vanishing derivatives, the following inequalities hold asymptotically:

$$\epsilon \geqslant O(\Delta x^{p+s-1}) \gg O(\Delta x^{2p}) \geqslant \tau_p,$$

which yields

$$\frac{\tau_p}{\epsilon + \beta^{(r)}} \ll 1. \tag{69}$$

By using Eq. (69), the weights can be recast as

$$w^{(r)} = \frac{d^{(r)} + d^{(r)} \frac{\tau_p}{\epsilon + \beta^{(r)}}}{1 + \sum_l \frac{\tau_p}{\epsilon + \beta^{(l)}}} = d^{(r)} + O\left(\frac{\tau_p}{\epsilon + \beta^{(r)}}\right), \tag{70}$$

where we use $\sum_r d^{(r)} = 1$. For any number of vanishing derivatives, we have

$$\frac{\tau_p}{\epsilon+\beta^{(r)}} \leqslant \frac{\tau_p}{\epsilon} \leqslant \frac{O(\Delta x^{2p})}{O(\Delta x^{p+s-1})} = O(\Delta x^{p-s+1}). \tag{71}$$

From Eq. (71) we see that $w^{(r)}$ converges to $d^{(r)}$ at the rate of $O(\Delta x^{p-s+1})$ or higher and satisfies the sufficient condition (41).

As mentioned at the beginning of this section, the two schemes that correspond to $\varphi = 0$ and $\varphi = \varphi_c$ require special consideration. Using the same procedure outlined above, it can easily be shown that if the parameter ϵ satisfies the following constraints:

$$\begin{aligned} &\epsilon \geqslant O(\Delta x^{3s-4}), \quad \text{for } \varphi = 0, \\ &\epsilon \geqslant O(\Delta x^{3s-3}), \quad \text{for } \varphi = \varphi_c, \end{aligned} \tag{72}$$

then the corresponding ESWENO schemes are design-order accurate regardless of the number of vanishing derivatives of the solution. The constraints (72) are derived using the following relations between the order of the scheme and the degree of the reconstruction polynomials:

$$\begin{aligned} &p = 2s-1, \quad \text{for } \varphi = 0, \\ &p = 2s, \quad \text{for } \varphi = \varphi_c. \end{aligned}$$

Also, note that if no constraint is imposed on ϵ except that it must be strictly positive, then the order of convergence of the pth-order WENO and ESWENO schemes with the new weights may deteriorate from p to $s+1$. Indeed, for a sufficiently large number of vanishing derivatives n_{vd}, $\beta^{(r)}$ and τ_p may become of the same order. For example, for the family of the fifth-order WENO and ESWENO schemes ($\varphi \neq 0$) with the new weight functions, this type of degeneration occurs at $n_{vd} = 4$. If $f' = f'' = f''' = f'''' = 0, f^{(5)} \neq 0$, and $\epsilon \leqslant O(\Delta x^{10})$ which *does not* satisfy the condition (62), then Eqs. (65) and (66) lead to

$$\frac{\tau_5}{\epsilon+\beta^{(r)}} = \frac{O(\Delta x^{10})}{O(\Delta x^{10}) + O(\Delta x^{10})} = O(1). \tag{73}$$

Using Eqs. (33), (34) and (73), the truncation error of the fifth-order ESWENO scheme at the critical point can be evaluated as follows:

$$\frac{\hat{f}_{j+1/2} - \hat{f}_{j-1/2}}{\Delta x} = \frac{h_{j+1/2} + c_5^+ f^{(5)} \Delta x^5 - h_{j-1/2} - c_5^- f^{(5)} \Delta x^5 + O(\Delta x^6)}{\Delta x} = \left.\frac{\partial f}{\partial x}\right|_{x_j} + O(\Delta x^4),$$

where $h_{j\pm1/2}$ is the numerical flux function given by Eq. (35). The above equation has been derived under the assumption that locally $f''' = f'''' = 0$, so that in Eq. (33), the third- and fourth-order terms vanish. Furthermore, $c_5^+ \neq c_5^-$, because at the critical point, the weight functions are far away from their preferred values, as follows from Eq. (73). As a result, the fifth-order WENO and ESWENO schemes with the new weights locally degenerate to fourth order, if the constraint (62) is not satisfied.

Remark 8. In [10], the following modification of the weight functions (17)–(19), (22) has been proposed to recover the fifth order of convergence if $n_{vd} \leqslant 2$:

$$w^{(r)} = \frac{\alpha_r}{\sum_l \alpha_l}, \quad \alpha_r = d^{(r)}\left[1 + \left(\frac{\tilde{\tau}_5}{\epsilon+\beta^{(r)}}\right)^m\right], \tag{74}$$

where $m = 2$. However, the modified weights (74) still experience the same degeneration in accuracy near critical points for any choice of the parameter m if $n_{vd} \geqslant 3$. A proof of this statement and a numerical example demonstrating this property are presented in Section 6.1.

Remark 9. The parameter ϵ is user-defined, and therefore, the sufficient conditions (62) and (72) can always be satisfied.

Remark 10. Eqs. (62) and (72) do not provide sharp estimates for the parameter ϵ, which can be weakened if additional information regarding the number of vanishing derivatives is available a priori. Note, however, that the constraints (62) and (72) guarantee the design order of convergence of the corresponding WENO and ESWENO schemes for smooth solutions with an arbitrary number of vanishing derivatives.

The last issue that we discuss in this section concerns discontinuous and unresolved solutions. To successfully emulate the ENO strategy, a stencil for which the solution is discontinuous should be eliminated from the approximation by effectively nullifying the corresponding weight that is associated with this stencil. Let a discontinuity be located inside a stencil S_r, while the solution is smooth in all other stencils. Since τ_p involves all points of the entire stencil including those containing the discontinuity, it is easy to verify that $\tau_p = O(1)$. Therefore, the weight $w^{(r)}$ can be evaluated as

$$w^{(r)} = \frac{d^{(r)}\left(1 + \frac{O(1)}{\epsilon+O(1)}\right)}{O(1) + \sum_{l\neq r} \frac{O(1)}{\epsilon+O(\Delta x^2)}} = \frac{O(1)}{O(1) + \frac{O(1)}{\epsilon+O(\Delta x^2)}} = O(1)\left(\epsilon + O(\Delta x^2)\right). \tag{75}$$

Based on the above equation, to reduce the influence of ϵ on the solution near the discontinuity, the parameter ϵ should satisfy the following constraint:

$$\epsilon \leqslant O(\Delta x^2). \tag{76}$$

Indeed, if Eq. (76) is met, then $w^{(r)}$ is of the order $O(\Delta x^2)$ and has the same order of magnitude as it would have if $\epsilon = 0$. Hence, the parameter ϵ must be bounded not only from below by Eqs. (62) and (72), but also from above by Eq. (76).

Another consideration that can help us optimally select the parameter ϵ is the manner in which the WENO and ESWENO schemes handle small-amplitude oscillations. Consider a solution that contains small-amplitude spurious oscillations

$$f = f_s + \delta f, \tag{77}$$

where f_s is a smooth component and δf is a nonsmooth, high-frequency component of the solution. Substituting Eq. (77) in Eq. (59) and assuming that the contribution of the smooth component is negligibly small, we have

$$\beta^{(r)} = O(\delta f^2).$$

As follows form Eq. (58), if $\epsilon \gg O(\delta f^2)$, then the denominator $\epsilon + \beta^{(r)}$ is dominated by ϵ, and these spurious oscillations cannot be detected by the ESWENO dissipation mechanism. However, if $\epsilon \leqslant O(\delta f^2)$, then the weights begin to deviate from their preferred values, which increases dissipation in those stencils containing spurious oscillations.

From these considerations it follows that the lower bound of the constraints on ϵ given by Eqs. (62), (72) and (76) should be used: (1) to obtain the design order of convergence at a smooth part of the solution, (2) to effectively damp high-frequency spurious oscillations, and (3) to provide good shock-capturing capabilities near strong discontinuities. Therefore, in our numerical experiments, we use

$$\epsilon = \begin{cases} O(\Delta x^{3s-4}), & \text{for } \varphi = 0, \\ O(\Delta x^{3s-3}), & \text{for } \varphi = \varphi_c, \\ O(\Delta x^{3s-2}), & \text{otherwise}, \end{cases} \tag{78}$$

where $s-1$ is the degree of the reconstruction polynomials. With the above selection of ϵ, all spurious oscillations of amplitude $O(\epsilon^{1/2})$ and higher are suppressed by the ESWENO dissipation mechanism. The same conclusions can be drawn for the WENO schemes with the new weights given by Eqs. (58)–(61).

6. Numerical results

We now assess the performance of the fourth-, fifth-, and sixth-order ESWENO schemes with the new weights and compare them with the conventional WENO counterparts. For all of the numerical experiments presented, the parameters ϵ of the ESWENO weight functions and the parameters δ_i of the additional artificial dissipation operator are chosen based on Eqs. (78) and (42) with two minor modifications. First, to preserve the scale invariance of the underlying linear schemes, the physical grid spacing Δx in Eqs. (42) and (78) is replaced with $\Delta\xi$, where $\Delta\xi = 1/J$ and J is the total number of grid cells. Second, as follows from Eq. (58), the parameter ϵ should be scaled consistently with $\beta^{(r)}$. In regions where the solution is smooth, for the third- and fourth-order WENO and ESWENO schemes, $\beta^{(r)}$ approximates $f'^2\Delta\xi^2$. For the fifth- and sixth-order schemes, $\beta^{(r)}$ approximates the linear combination of the same first-order derivative term and a second-order derivative term that is proportional to f''^2. The same pattern persists for higher order schemes as well. In the vicinity of discontinuities, $\beta^{(r)}$ is of the order of $O(f^2)$. Taking into account the above considerations, for all test problems considered the parameter ϵ is set to

$$\epsilon = \begin{cases} C\Delta\xi^{3s-4}, & \text{for } \varphi = 0, \\ C\Delta\xi^{3s-3}, & \text{for } \varphi = \varphi_c, \\ C\Delta\xi^{3s-2}, & \text{otherwise}, \end{cases} \qquad C = \max_{\xi \neq \xi_d} \left(\|f_0'^2\|, \|f_0'^2\|, \ldots, \|(f_0^{(s-1)})^2\| \right), \tag{79}$$

where $f_0 = f(u_0(\xi))$ is the initial flux, $u_0(\xi)$ is the initial condition, $f_0^{(s-1)}$ is the $(s-1)$th-order derivative of f_0 with respect to ξ, $(s-1)$ is the degree of the reconstruction polynomials, ξ_d is a set of points at which the solution is discontinuous, and $\|\cdot\|$ is a norm in which the solution is sought. The derivatives of f_0 in Eq. (79) are computed numerically. The scaling factor C in Eq. (79) can easily be evaluated because it depends only on the initial condition for which the locations of all discontinuities are known a priori. The parameter ϵ is calculated once and the same value is used over the entire time interval of integration; thus the computational cost does not increase. Note, however, that if the initial condition is zero and the solution of the governing equation is mostly determined by a source term, then the scaling factor and the parameter ϵ given by Eq. (79) become equal to zero. This problem can be overcome by using the following simple strategy. Initially, the computation starts with some nonzero value of C (e.g., $C = 1$). After several time steps when the solution significantly deviates from its initial condition, the parameter ϵ is recomputed using Eq. (79) with the solution obtained at the current time level. In principle, the parameter ϵ should be updated every time when the norm of the solution or its derivatives changes significantly, i.e., by a factor of $O(1/\Delta\xi)$. It is unlikely that such significant changes may occur frequently, thus making us to believe that the

parameter ϵ should be updated only a few times (possibly once) over the entire time interval of integration. An approach similar to Eq. (79) for calculating the parameter ϵ can also be used for systems of equations. For hyperbolic systems, a separate set of weight functions as well as a separate parameter ϵ are computed for each component of the characteristic variables. In other words, for the mth component of the characteristic variables, the corresponding tuning parameter ϵ_m is computed using Eq. (79) with $f_0 = \mathbf{l}_m^T \mathbf{U}_0$, where $\mathbf{l}_m$ is the mth left eigenvector of the Jacobian of this hyperbolic system, and $\mathbf{U}_0$ is the vector of conserved variables at $t = 0$.

In accordance with Eq. (23), the parameter δ_i should be scaled consistently with λ_i. Because λ_i is a linear combination of the weights with each being of the order $O(1)$, the scaling factor of δ_i is set equal to one, which leads to

$$\delta_i = \Delta\xi^{p-2i+1}. \tag{80}$$

Eqs. (79) and (80) eliminate the ambiguity in determining the parameters ϵ and δ_i for the ESWENO schemes, thus making them free of tuning parameters. Furthermore, Eqs. (79) and (80) are fully consistent with the sufficient conditions (42) and (78) and provide that the ESWENO schemes are invariant when the spatial and time variables are scaled by the same factor.

Along with the conventional WENO schemes proposed in [2,8], the fifth-order WENO-Z scheme developed in [10], and the new ESWENO schemes, we also consider the conventional WENO schemes with the new weight functions given by Eqs. (58)–(61), which are referred as WENO-NW. Note that the parameter ϵ for the conventional WENO schemes is set to be 10^{-6} as recommended in [2]. In accordance with the recommendations of Borges et al. [10], the parameter ϵ for the fifth-order WENO-Z scheme with the weights given by Eqs. (17)–(19), (22) is set to 10^{-40}. For the WENO-NW schemes, the parameter ϵ is computed using Eq. (79).

The time derivative for all steady test problems is approximated by using a third-order total variation diminishing (TVD) Runge–Kutta method developed in [14], while unsteady problems are integrated by using a fourth-order low-storage Runge–Kutta method [15]. To reduce the fourth-order temporal error component and make it consistent with the spatial error of fifth- and sixth-order schemes, the time step in global grid refinement studies is reduced by a factor of $2^{6/4}$ for each doubling of the number of grid points in space. The Courant–Friedrich–Levy (CFL) number has been set equal to 0.3 and 0.6 for the steady and unsteady test problems, respectively.

6.1. Scalar linear wave equation

We begin by verifying that the new class of ESWENO schemes provide the design order of convergence for smooth problems, including local extrema. To check this property, we consider Eq. (1) with $a = 1$ and the following initial condition:

$$u_0(x) = e^{-300(x-x_c)^2}, \tag{81}$$

where x_c is 0.5. The computational domain for this test problem is set to $0 \leqslant x \leqslant 1$. Numerical solutions are calculated on a sequence of globally refined uniform grids and advanced in time up to $t = 1$, which corresponds to one period in time.

First, we show that the conventional fourth-order WENO scheme is unstable for this smooth problem; however, the corresponding ESWENO is stable, and its solution is in excellent agreement with the exact solution, as one can see in Fig. 2. To make the conventional fourth-order WENO scheme stable, a smoothness indicator corresponding to the downwind stencil has been modified as follows:

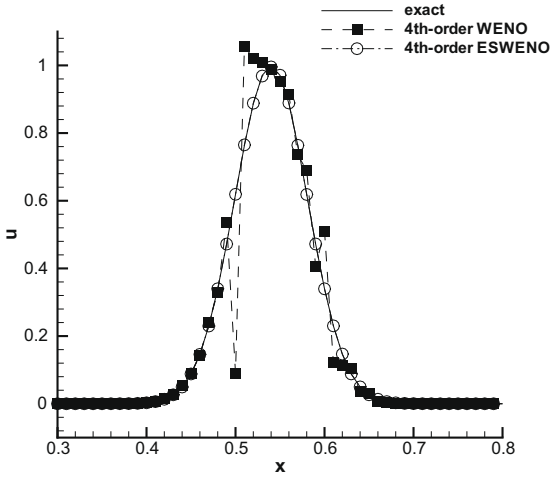

Fig. 2. Solutions obtained with the fourth-order WENO and ESWENO schemes on a 101-point grid for the linear wave equation with the initial condition (81) at $t = 0.04$.

$$\bar{\beta}^R = \left[\frac{(\beta^L)^k + (\beta^C)^k + (\beta^R)^k}{3}\right]^{1/k}, \tag{82}$$

where k is a constant that is greater than 1. Note that $\bar{\beta}^R$ is a C^∞ function of its arguments and approaches $\max(\beta^L, \beta^C, \beta^R)$ as $k \to \infty$. In contrast to Eq. (82), a modified smoothness indicator $\bar{\beta}^R = \max(\beta^L, \beta^C, \beta^R)$ proposed in [8] is a nonsmooth function of β^L, β^C and β^R, which may lead to the degeneration of the design order of accuracy and is more prone to spurious oscillations near unresolved features and strong discontinuities. For $k \to \infty$, the downwind smoothness indicator given by Eq. (82) prevents the corresponding weight w^R from being larger than the lesser of the other two weight functions; thus, the stencil is biased in the upwind direction near unresolved features. In smooth regions, all three smoothness indicators are of the same order, and the weights approach their preferred values $w^L = \frac{1}{6}, w^C = \frac{2}{3}$, and $w^R = \frac{1}{6}$, which provides the design order of accuracy. For all the numerical experiments that are presented herein, the parameter k in Eq. (82) is set equal to 4.

Fig. 3 shows L_∞ error norms obtained with the fourth-order WENO, WENO-NW, ESWENO, and the corresponding underlying linear schemes. As shown in Fig. 3, the fourth-order ESWENO scheme is significantly more accurate than the conventional fourth-order WENO scheme. The L_∞ error obtained with the fourth-order ESWENO scheme is slightly higher than that obtained with the corresponding linear scheme on coarse meshes and reaches its theoretical limit starting at $J = 200$ grid cells. The maximum error occurs at the peak of the Gaussian pulse indicating that the ESWENO scheme is design-order accurate at the smooth extremum. In contrast to the ESWENO scheme, the conventional WENO scheme demonstrates only a third-order convergence rate, even on the finest mesh with $J = 1600$, and is two to three orders of magnitude less accurate on moderate and fine meshes.

If the new weights (58) and (59) are used instead of their conventional counterparts, then the design order of convergence of the fourth-order central WENO scheme is recovered, as shown in Fig. 3. Moreover, the fourth-order WENO-NW scheme provides slightly better accuracy on coarse meshes than the corresponding ESWENO scheme. This result is not surprising because the ESWENO scheme has the additional dissipation term (24), which guarantees the stability. In general, if a WENO-NW scheme is stable, then it is slightly less dissipative than the corresponding ESWENO counterpart.

The L_∞ error norms obtained with the fifth-order WENO-Z scheme and the fifth- and sixth-order WENO and ESWENO schemes for the same test problem are depicted in Fig. 4. Similar to the fourth-order case, the conventional sixth-order central WENO scheme is unstable. This problem is avoided by using the same upwinding technique that is outlined earlier. For the sixth-order central WENO scheme, the modified smoothness indicator that corresponds to the most downwind stencil is given by

$$\bar{\beta}^{RR} = \left[\frac{(\beta^{LL})^k + (\beta^L)^k + (\beta^R)^k + (\beta^{RR})^k}{4}\right]^{1/k}. \tag{83}$$

Both the fifth-order WENO-Z and fifth- and sixth-order ESWENO schemes are equal in accuracy to the corresponding underlying linear schemes, as shown in Fig. 4. Although the fifth-order WENO scheme exhibits the design-order convergence rate, its L_∞ error norm is nearly an order of magnitude larger than those of the corresponding fifth-order WENO-Z and ESWENO schemes. In contrast to the L_∞ error of the sixth-order ESWENO scheme, the L_∞ error obtained with the conventional sixth-order WENO scheme shows only fifth-order convergence and is quite far from the theoretical limit represented by the corresponding sixth-order central linear scheme. Note that fourth- and sixth-order WENO-Z schemes are currently unavailable in the published literature and therefore are not presented herein.

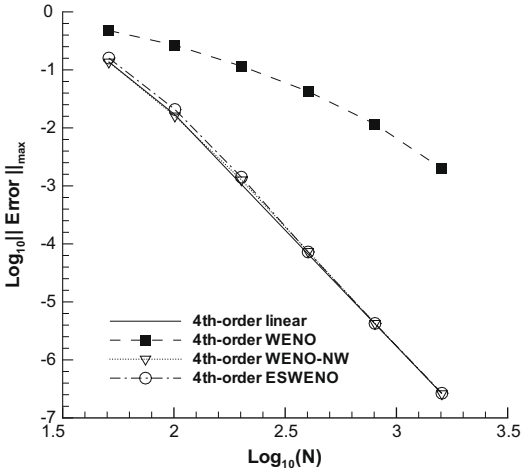

Fig. 3. L_∞ error norms obtained with the fourth-order linear, WENO, WENO-NW, and ESWENO schemes for linear wave equation with initial condition (81).

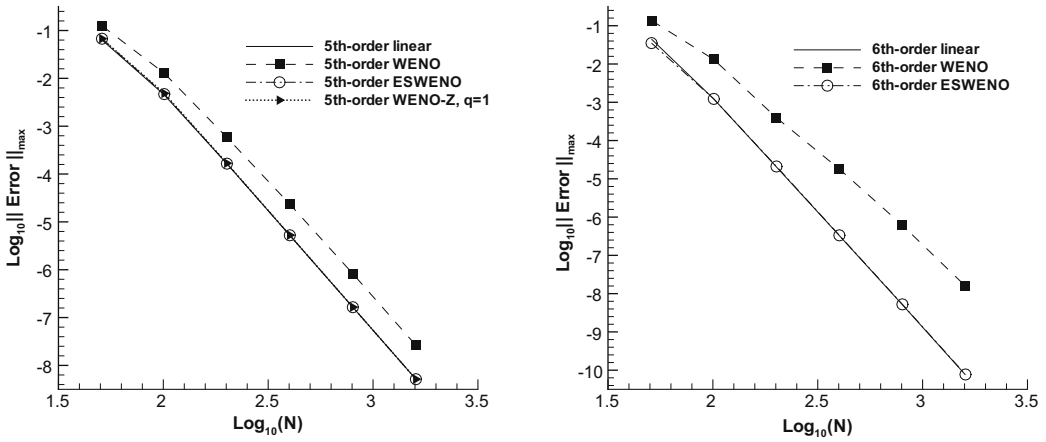

Fig. 4. L_∞ error norms obtained with the fifth-(left) and sixth-order (right) linear, WENO, WENO-Z, and ESWENO schemes for linear wave equation with initial condition (81).

Table 1
The CPU time (in seconds) required by the WENO and ESWENO schemes for integration of the linear wave equation with initial condition (81) over 5 periods on 101-point mesh.

Scheme	Third-order	Fourth-order	Fifth-order	Sixth-order
WENO	0.34	0.67	1.56	2.11
ESWENO	0.41	0.95	1.80	2.52

We now evaluate the computational overhead caused by the ESWENO additional artificial dissipation term given by Eq. (24). Table 1 shows the amount of CPU time required by the third- to sixth-order WENO and ESWENO schemes to integrate Eq. (1) with the initial condition (81) over 5 periods on a 101-point grid. Because the third- and fifth-order schemes are fully upwind biased, the most downwind stencil is not used in the approximation, thus reducing the computational cost as compared with the fourth- and sixth-order schemes. For the numerical schemes presented in Table 1, the maximum relative increase in the computational cost occurs for the fourth-order ESWENO scheme. The third-, fifth-, and sixth-order ESWENO schemes are only 15–20% more expensive in terms of the computational time as compared with the corresponding WENO counterparts. Based on the results presented in the table and the comparison of the WENO and ESWENO fluxes, we can conclude that no appreciable increase in the relative computational overhead is expected for higher order schemes. Note that no attempts have been made to optimize the implementation of both the WENO and ESWENO schemes.

As has been proven in Sections 2 and 4.1, for the linear convection Eq. (1) with piecewise continuous initial conditions, the family of ESWENO schemes is stable in the energy norm. The sufficient condition for stability is the negative semidefiniteness of $-\frac{1}{2}(\overline{D}+\overline{D}^T)$, where $\overline{D}$ is the ESWENO discrete operator. This property implies that all eigenvalues of the symmetric part of the ESWENO operator are nonpositive. In contradistinction to the ESWENO scheme, the symmetric part of the WENO operator may have positive eigenvalues, as has been shown in Section 4.1. Note that the same conclusion can be drawn for the fifth-order WENO-Z scheme [10], whose derivative operator is identical to that of the conventional WENO scheme with the modified weights (17)–(19), (22) which vary in the interval from 0 to 1 near the unresolved features. These properties of the WENO, WENO-Z, and ESWENO schemes are shown in Fig. 5, which gives the time histories of the rightmost eigenvalue of the symmetric part of the operators computed on a 201-point grid. The rightmost eigenvalue of the ESWENO operator $-\frac{1}{2}(\overline{D}+\overline{D}^T)$ is equal to zero to the order of the round-off error, while the symmetric part of the conventional fifth-order WENO and WENO-Z operators have positive eigenvalues of order $O(10^{-1})$ and $O(10)$, respectively, as one can see in Fig. 5. This is due to the fact that the symmetric part of these WENO-type operators is not negative semidefinite, if there are unresolved features in the computational domain. Note that the presence of the positive eigenvalues *does not* imply that the fifth-order WENO and WENO-Z schemes are globally unstable because these eigenvalues correspond to different grid points at different moments of time.

The superiority of the ESWENO schemes with the new weights as compared with the conventional and modified WENO counterparts becomes evident when a more challenging problem is considered. In the previous test problem, the initial condition (81) has the critical point at which $f'=0$ and $f''\neq 0$ (i.e., the number of vanishing derivatives $n_{vd}=1$). We now show that the fifth-order WENO-Z scheme developed by Borges et al. [10] fails to recover the design order of convergence if $n_{vd}\geqslant 3$ for an arbitrary choice of the parameter m in Eq. (74). Consider Eq. (1) with the following initial condition:

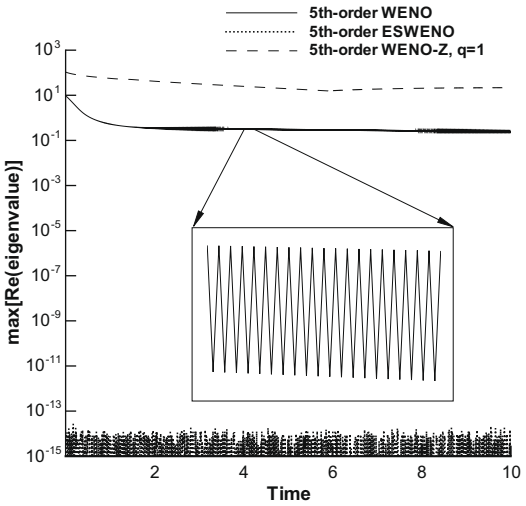

Fig. 5. Time histories of the rightmost eigenvalue of the symmetric part of fifth-order WENO and ESWENO operators for the Gaussian pulse problem.

$$u_0(x) = \begin{cases} z^{18} - 14z^{16} + 69z^{14} - 175z^{12} + 259z^{10} \\ -231z^8 + 119z^6 - 29z^4 + 1, & \text{for } |z| \leqslant 1 \\ 0, & \text{otherwise} \end{cases} \tag{84}$$

where $z = 5(x - 0.5)$ and $0 \leqslant x \leqslant 1$. The above function is six times continuously differentiable and has three critical points: one at $x = 0.5$ with $n_{vd} = 3$ (i.e., $f'(0.5) = f''(0.5) = f'''(0.5) = 0$ and $f''''(0.5) \neq 0$) and the remaining two at $x = 0.3$ and 0.7 with $n_{vd} = 6$. If we compare the L_∞ error norms computed with the fifth-order linear, WENO, WENO-Z, and ESWENO schemes at $t = 1$ (see Fig. 6), we see that the situation changes dramatically as compared with the previous test problem. As expected, the WENO-Z scheme fails to deliver fifth order of convergence, while the ESWENO scheme is fifth-order accurate and provides practically the same error convergence as the underlying linear scheme. This result is not surprising because the parameter ϵ for the WENO-Z scheme is set to 10^{-40}, as suggested in [10]. As a result, the weights at point $x_j = 0.5 + \Delta x$ become of order O(1), thus leading to the degeneration in the order of convergence for any choice of the parameter m in Eq. (74). Indeed, using Eqs. (65), (22), (74) with $\epsilon = 0$ and taking into account that for the polynomial in Eq. (84), $f_j' = O(\Delta x^3), f_j'' = O(\Delta x^2), f_j''' = O(\Delta x)$, and $f_j'''' = O(1)$ at $x_j = 0.5 + \Delta x$, we have

$$w^{(r)} - d^{(r)} = O\left(\left[\frac{|\frac{13}{3} f_j'' f_j''' - f_j' f_j''''| \Delta x^5}{f_j'^2 \Delta x^2 + (\frac{13}{3} f_j'^2 - f_j' f_j''') \Delta x^4}\right]^m\right) = \left(\frac{O(\Delta x^8)}{O(\Delta x^8)}\right)^m = O(1). \tag{85}$$

Using Eqs. (33), (34), (85), the truncation error of the WENO-Z scheme at $x_j = 0.5 + \Delta x$ can be evaluated as follows:

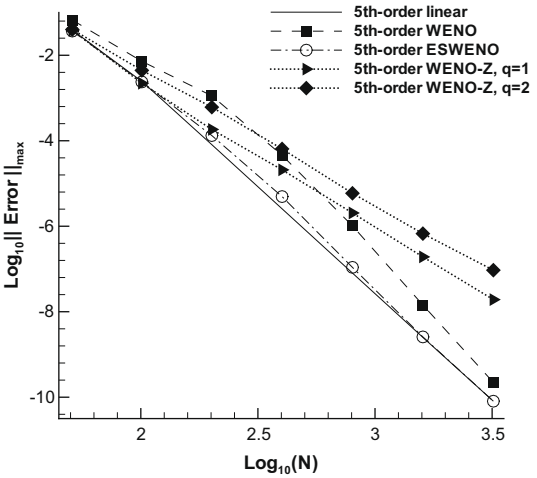

Fig. 6. L_∞ error norms obtained with fifth-order linear, WENO, WENO-Z, and ESWENO schemes for linear wave equation with initial condition (84) at $t = 1$.

$$\frac{\hat{f}_{j+1/2}-\hat{f}_{j-1/2}}{\Delta x}=\frac{h_{j+1/2}+c_3^+f'''\Delta x^3-h_{j-1/2}-c_3^-f'''\Delta x^3+O(\Delta x^4)}{\Delta x}=\left.\frac{\partial f}{\partial x}\right|_{x_j}+O(f'''\Delta x^2)=\left.\frac{\partial f}{\partial x}\right|_{x_j}+O(\Delta x^3),$$

where $h_{j\pm1/2}$ is the numerical flux function given by Eq. (35), the coefficients c_3^+ and c_3^- depend on the weight functions but do not depend on Δx and are not equal to each other because Eq. (85) holds. As follows from the above estimate, the WENO-Z scheme locally degenerates to third order regardless of the choice of the parameter m in Eq. (74). Our numerical results corroborate this conclusion. Fig. 6 shows that increasing the exponent m in Eq. (74) results in an even larger deterioration in accuracy. In contrast to the WENO-Z scheme, the conventional fifth-order scheme of Jiang and Shu converges at the design order and begins to approach the theoretical limit on finest meshes. The main reason for such a behavior is the choice of the parameter ϵ, which is set to 10^{-6}. As the grid is refined, the sufficient condition on ϵ given by Eq. (62) is satisfied on sufficiently fine meshes, and the conventional WENO scheme becomes design-order accurate.

6.2. The 1-D Euler equations

In [1], the third-order ESWENO scheme is proved to be energy stable for a system of linear hyperbolic equations with periodic boundary conditions. This result can be directly extended to the class of higher order ESWENO schemes that are presented in this paper. For nonlinear conservation laws with nonperiodic boundary conditions, a similar proof for the high-order ESWENO schemes is not currently available. Nevertheless, we would like to test how the new schemes perform for the system of the quasi-1-D Euler equations, which are given by

$$\begin{aligned}&\frac{\partial \mathbf{U}}{\partial t}+\frac{\partial \mathbf{F}}{\partial x}=\mathbf{G},\\ &\mathbf{U}=\begin{bmatrix}\rho\\ \rho u\\ E\end{bmatrix},\quad \mathbf{F}=\begin{bmatrix}\rho u\\ \rho u^2+P\\ (E+P)u\end{bmatrix},\quad \mathbf{G}=-\frac{A_x}{A}\begin{bmatrix}\rho u\\ \rho u^2\\ (E+P)u\end{bmatrix},\\ &P=(\gamma-1)\left(E+\frac{\rho u^2}{2}\right),\end{aligned}\tag{86}$$

where $A=A(x)$ is the cross-sectional area of a quasi-1-D nozzle and $\gamma=1.4$. As has been shown in [1], the ESWENO reconstruction must be implemented in local characteristic fields to guarantee the stability of the ESWENO scheme for systems of hyperbolic conservation laws. In the present analysis, both the WENO and ESWENO reconstructions are based on the Lax–Friedrichs flux splitting. See [1] for further details.

For the 1-D Euler equations, the preferred biasing of the stencil in the upwind direction, given by Eqs. (82) and (83), is used for the central fourth- and sixth-order WENO and ESWENO schemes to suppress spurious oscillations near strong discontinuities. In the ESWENO case, these oscillations can also be eliminated by increasing the coefficient in front of the $D_1\Lambda_1D_1^T$ term in the artificial dissipation operator. However, this approach is more dissipative and also reduces the maximum CFL number for which the scheme remains stable.

To verify that the new ESWENO schemes are design-order accurate for hyperbolic systems, we consider the steady-state isentropic flow through a quasi-1-D nozzle with the following cross-sectional area: $A(x)=1-0.8x(1-x)$, $0\leqslant x\leqslant 1$ as a test problem. The inflow Mach number is set to 0.5 and the pressure at $x=1$ is assumed to be equal to that at $x=0$. Under these conditions, the flow is fully subsonic, and the solution is smooth. Global grid refinement studies for the third-, fourth-, fifth-, and sixth-order WENO and ESWENO schemes are presented in Fig. 7.

The L_∞ error norms obtained with the third- and fourth-order ESWENO schemes exhibit the design order of convergence. On the finest mesh with $J=800$, the fourth-order ESWENO solution is approximately three and four orders of magnitude more accurate than those of the third-order ESWENO and WENO schemes, respectively. As shown in Fig. 7, the fifth-order ESWENO scheme provides the same accuracy as its underlying linear scheme, thereby exhibiting the perfect error convergence for this test problem. Although the conventional fifth-order WENO scheme exhibits the design order of convergence, its L_∞ error norm is larger by a factor of 3 than that obtained with the ESWENO counterpart. Similar to the forth-order case, the central sixth-order ESWENO scheme converges at the design-order rate on both coarse and fine meshes, thus providing significantly more accurate solutions than both fifth-order schemes.

Remark 11. For this problem, the conventional central fourth- and sixth-order WENO schemes do not converge to a steady-state solution even with the upwinding mechanisms (82) and (83) turned on. The primary reason for such a behavior is the presence of positive eigenvalues in the spectrum of the symmetric part of the conventional WENO operator.

The next test problem is the steady transonic flow through a quasi-1-D nozzle with the following cross-sectional area:

$$A(x)=1.398+0.347\tanh(0.8x-4),\quad 0\leqslant x\leqslant 10.$$

The Mach number at $x=0$ is 1.5, and the outflow conditions have been chosen so that the shock is located at $x=5$. Density profiles calculated using the fifth-order WENO and fifth- and sixth-order ESWENO schemes on a 51-point grid are compared with the exact solution in Fig. 8. For all schemes, the captured shock is smeared over two grid cells, and the numerical solu-

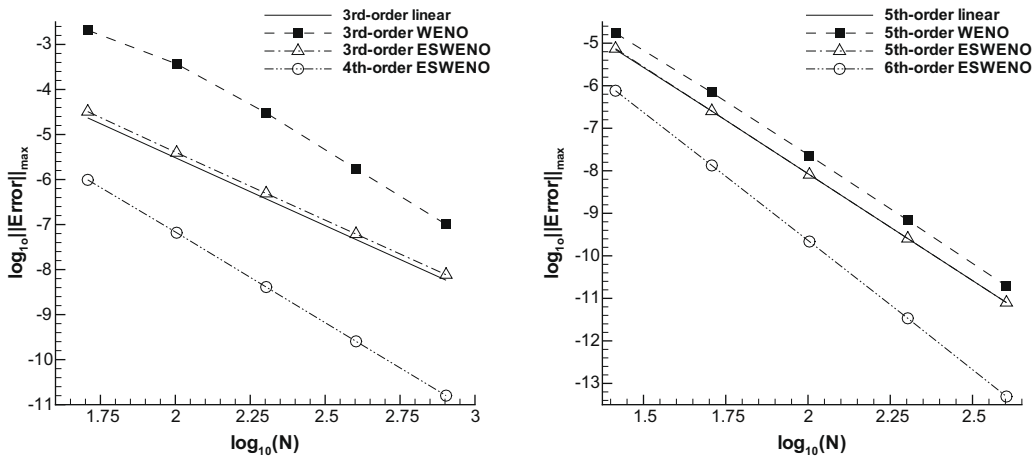

Fig. 7. L_∞ error norms obtained with the third- and fourth-order (left) and fifth- and sixth-order linear and WENO, ESWENO schemes for the subsonic quasi-1-D nozzle problem.

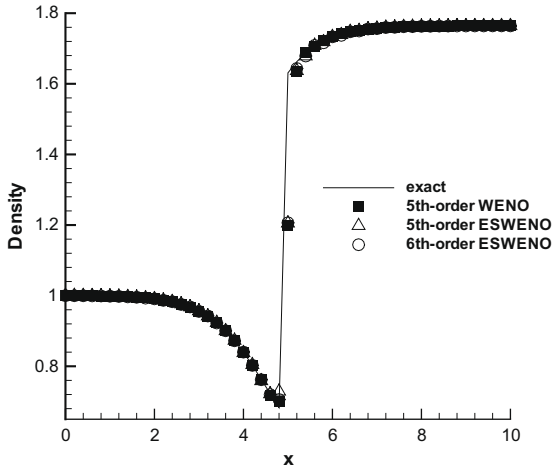

Fig. 8. Comparison of fifth-order WENO and ESWENO schemes for the steady transonic flow through quasi-1-D nozzle.

tions are essentially non-oscillatory and agree quite well with the exact solution. Note that the fifth- and sixth-order ESWENO schemes converge to the steady-state solution an order of magnitude faster than the conventional fifth-order WENO scheme. Furthermore, the residual of the fifth-order WENO-Z scheme for this steady state problem levels out at 10^{-2} and cannot be driven below this level. These results again indicate the presence of unstable modes that are generated by the positive eigenvalues of the WENO dissipation operator.

The last two problems considered are standard unsteady problems for testing shock-capturing schemes. The first one is the Riemann problem with the following initial conditions:

$$(\rho, u, P) = \begin{cases} (1, 0, 1) & \text{if } -0.5 \leqslant x < 0, \\ (0.125, 0, 0.1) & \text{if } 0 \leqslant x \leqslant 0.5, \end{cases}$$

which were proposed by Sod. The numerical solutions computed with the fourth- and sixth-order ESWENO and conventional WENO schemes are depicted in Fig. 9. To evaluate the amount of dissipation introduced by the additional ESWENO dissipation operator (24), we also present the density profiles obtained with the fourth- and sixth-order WENO-NW scheme. In the fourth-order case, all the solutions are essentially non-oscillatory, as one can see in Fig. 9. Note, however, that the ESWENO and WENO-NW schemes provide better resolution near the contact discontinuity as compared with the conventional WENO scheme. In contrast to the fourth-order case, the 6th-order WENO-NW scheme exhibits spurious oscillations near the contact discontinuity, whereas the solutions of the ESWENO scheme with the same weight functions and the conventional WENO scheme are free of spurious oscillations. This comparison shows that the ESWENO dissipation operator plays a very important role and eliminates the unstable modes present in the conventional WENO dissipation operator. As in the previous test case, the sixth-order ESWENO scheme is less dissipative than its conventional counterpart.

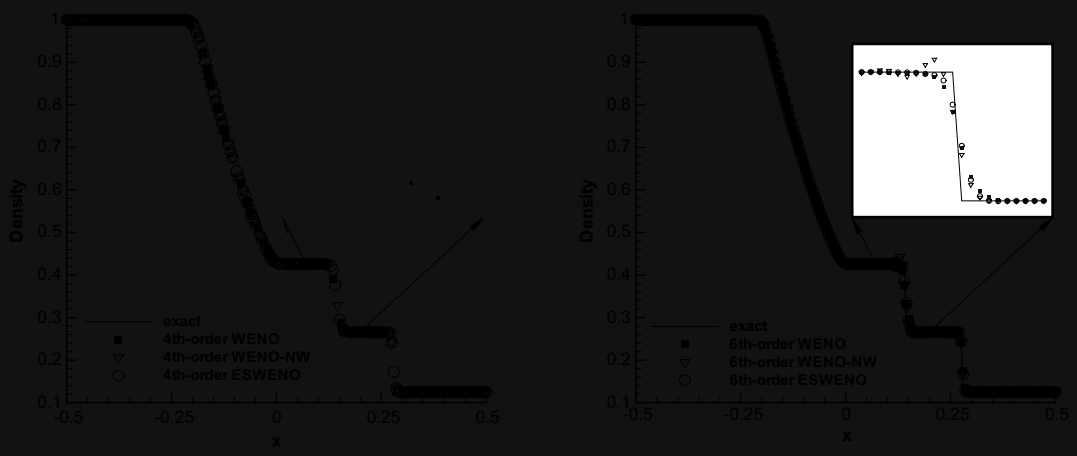

Fig. 9. Density profiles computed with the fourth-order (left) and sixth-order (right) ESWENO schemes and the WENO schemes with standard and new

structures, and is well suited for testing high-order shock-capturing schemes. The governing equations are the time-dependent 1-D Euler equations (86) with $\mathbf{G} = \mathbf{0}$, subject to the following initial conditions:

$$(\rho, u, p) = \begin{cases} (3.857134, 2.629369, 10.33333), & \text{if } -5 \leqslant x < -4, \\ (1 + 0.2\sin 5x, 0, 1), & \text{if } -4 \leqslant x \leqslant 5. \end{cases} \tag{87}$$

The governing equations are integrated in time up to $t = 1.8$. The exact solution to this problem is not available. Therefore, a

Appendix A. *A.1. Existence of symmetric decomposition*

The following lemma establishes the existence of the decomposition $D_{sym} = \sum_{i=0}^{s} [D_1^i] \Lambda_i [D_1^i]^T$. The lemma provides an algorithm to decompose a matrix of arbitrary bandwidth $2s+1$ into the sum of two matrices: one that can be expressed as one term of the desired symmetric form, and one of bandwidth $2(s-1)+1$.

Lemma 1. *Define E_s to be an N-dimensional, symmetric, bidiagonal matrix with the subdiagonal elements $e_{s+1,1}$, $e_{s+2,2}, \ldots, e_{N-1,N-s-1}$, $e_{N,N-s}$. The parameter s is the offset from the main diagonal. Further, define B_{s-1} to be an N-dimensional, symmetric, banded matrix of bandwidth $2(s-1)+1$ with elements that are functions of the matrix E_s. The matrices E_s and B_{s-1} satisfy the following relationship:*

$$E_s = (-1)^s [D_1^s] \Lambda_s [D_1^s]^T + B_{s-1},$$

with $\Lambda_s = diag[e_{s+1,1}, e_{s+2,2}, \ldots, e_{N-1,N-s-1}, e_{N,N-s}, \mathbf{0}_s^T]$ and $\mathbf{0}_s$ is a zero vector of dimension s.

Proof. A proof by induction is not included herein. One step of the algorithm can be verified immediately by inspection.

A simple example illustrates Lemma 1. Define the 5×5 matrices E_2, D_{15}, and B_1 such that $E_2 = (-1)^2 [D_{15}^2] \Lambda_2 [D_{15}^2]^T + B_1$ and

$$E_2 = \begin{pmatrix} 0 & 0 & a & 0 & 0 \\ 0 & 0 & 0 & b & 0 \\ a & 0 & 0 & 0 & c \\ 0 & b & 0 & 0 & 0 \\ 0 & 0 & c & 0 & 0 \end{pmatrix}; \quad D_{15} = \begin{pmatrix} 1 & 0 & 0 & 0 & -1 \\ 1 & 1 & 0 & 0 & 0 \\ 0 & -1 & 1 & 0 & 0 \\ 0 & 0 & -1 & 1 & 0 \\ 0 & 0 & 0 & -1 & 1 \end{pmatrix},$$

$$\Lambda_2 = \begin{pmatrix} a & 0 & 0 & 0 & 0 \\ 0 & b & 0 & 0 & 0 \\ 0 & 0 & c & 0 & 0 \\ 0 & 0 & 0 & 0 & 0 \\ 0 & 0 & 0 & 0 & 0 \end{pmatrix}; \quad B_1 = \begin{pmatrix} a & -2a & 0 & 0 & 0 \\ 2a & 4a+b & -2(a+b) & 0 & 0 \\ 0 & -2(a+b) & a+4b+c & -2(b+c) & 0 \\ 0 & 0 & -2(b+c) & b+4c & -2c \\ 0 & 0 & 0 & -2c & c \end{pmatrix} \quad \square$$

Remark 12. Lemma 1 can be used recursively, beginning with the outermost s diagonal and working inward, to establish that $D_{sym} = \sum_{i=0}^{s} [D_1^i] \Lambda_i [D_1^i]^T$. Each step generates a new symmetric matrix with a bandwidth that is equal to 2 less than the previous value until only a diagonal matrix remains. Thus, the algorithm terminates after $s+1$ steps with the desired decomposition.

Remark 13. This recursive algorithm works for nonperiodic matrices in multiple spatial dimensions.

A.2. Third- and fourth-order ESWENO schemes

Based on Eq. (13), $\hat{f}_{j+\frac{1}{2}}$ defined for a family of third-order WENO schemes is

$$\hat{f}_{j+\frac{1}{2}} = w_{j+1/2}^L f_{j+1/2}^L + w_{j+1/2}^C f_{j+1/2}^C + w_{j+1/2}^R f_{j+1/2}^R, \tag{88}$$

where w^L, w^C, and w^R are weight functions that are assigned to each respective stencil. The second-order linear fluxes: $f_{j+1/2}^{(r)}$, defined in Eq. (88) for $r = \{L, C, R\}$, are:

$$\begin{pmatrix} f^L(u_{j+1/2}) \\ f^C(u_{j+1/2}) \\ f^R(u_{j+1/2}) \end{pmatrix} = \frac{1}{2} \begin{pmatrix} -1 & 3 & 0 & 0 \\ 0 & 1 & 1 & 0 \\ 0 & 0 & 3 & -1 \end{pmatrix} \begin{pmatrix} f(u_{j-1}) \\ f(u_j) \\ f(u_{j+1}) \\ f(u_{j+2}) \end{pmatrix}. \tag{89}$$

The terms w^L, w^C, and w^R are the nonlinear weight functions given by Eqs. (58) and (59) with

$$\tau_3 = \begin{cases} (-f_{j-1} + 3f_j - 3f_{j+1} + f_{j+2})^2, & \text{for } \varphi \neq 0 \\ (f_{j-1} - 2f_j + f_{j+1})^2, & \text{for } \varphi = 0 \end{cases}$$

(see [1] for further details). These weight functions have preferred values that are derived from underlying linear schemes, as well as solution dependent components. The preferred values are given by the formulae

$$d_{:}^{L} = \frac{1}{3} - \varphi; \quad d_{:}^{C} = \frac{2}{3}; \quad d_{:}^{R} = \varphi, \tag{90}$$

where φ is a parameter. The convergence rate of Eq. (13) with the preferred weight values given by Eq. (88) is equal to 3 for all values of the parameter φ except $\varphi_c = \frac{1}{6}$, for which the convergence rate is 4.

Combining Eq. (89) with Eq. (88) and substituting the resulting WENO flux $\hat{f}_{j+\frac{1}{2}}$ into Eq. (13) produces a stencil for the jth grid point of the form

$$D^3_{j,:} = \frac{1}{2\Delta x}\left(\begin{array}{c|c|c|c|c} 0 & -w^L_{j+1/2} & 3w^L_{j+1/2} & 0 & 0 \\ 0 & 0 & w^C_{j+1/2} & w^C_{j+1/2} & 0 \\ 0 & 0 & 0 & 3w^R_{j+1/2} & -w^R_{j+1/2} \\ w^L_{j-1/2} & -3w^L_{j-1/2} & 0 & 0 & 0 \\ 0 & -w^C_{j-1/2} & -w^C_{j-1/2} & 0 & 0 \\ 0 & 0 & -3w^R_{j-1/2} & w^R_{j-1/2} & 0 \end{array}\right)\begin{pmatrix} f(u_{j-2}) \\ f(u_{j-1}) \\ f(u_j) \\ f(u_{j+1}) \\ f(u_{j+2}) \end{pmatrix} \tag{91}$$

Simplifying D^3 using the expression

$$w_{:}^{C} = 1 - w_{:}^{L} - w_{:}^{R}$$

yields expressions for a single row of the D^3 matrix of the following form:

$$D^3_{j,:} = \frac{1}{2\Delta x}\begin{pmatrix} \vdots \\ 0 \\ w^L_{j-1/2} \\ -2w^L_{j-1/2} - w^L_{j+1/2} + w^R_{j-1/2} - 1 \\ w^L_{j-1/2} + 2w^L_{j+1/2} - 2w^R_{j-1/2} - w^R_{j+1/2} \\ -w^L_{j+1/2} + w^R_{j-1/2} + 2w^R_{j+1/2} + 1 \\ -w^R_{j+1/2} \\ 0 \\ \vdots \end{pmatrix}^T. \tag{92}$$

The derivative matrix D^3 is now decomposed into symmetric and skew-symmetric parts

$$D^3 = D^3_{skew} + D^3_{sym}.$$

As with the fifth-order case, the skew-symmetric component of D^3 takes the form

$$D^3_{skew} = P^{-1}Q_3; \quad Q_3 + Q_3^T = 0; \quad P = \Delta x I,$$

while the matrix D^3_{sym} is expressed as

$$D^3_{sym} = P^{-1}\left(D^2_1 \Lambda^3_2 [D^2_1]^T + D^1_1 \Lambda^3_1 [D^1_1]^T + D^0_1 \Lambda^3_0 [D^0_1]^T\right), \tag{93}$$

where $\Lambda^3_{:}$ is a diagonal matrix with the expressions for the jth element defined by

$$(\lambda^3_2)_{jj} = \frac{1}{4}\left[w^L_{j+3/2} - w^R_{j+1/2}\right], \tag{94}$$

$$(\lambda^3_1)_{jj} = \frac{1}{4}\left[-w^L_{j+3/2} + w^L_{j+1/2} - w^R_{j+1/2} + w^R_{j-1/2}\right], \tag{95}$$

$$(\lambda^3_0)_{jj} = \frac{1}{2}\left[-w^L_{j-1/2} - w^C_{j-1/2} - w^R_{j-1/2} + w^L_{j+1/2} + w^C_{j+1/2} + w^R_{j+1/2}\right] = 0. \tag{96}$$

Defining $(\bar{\lambda}^3_i)_{jj}, i = \overline{1,2}$ to be smoothly positive

$$(\bar{\lambda}^3_i)_{jj} = \frac{1}{2}[\sqrt{(\lambda^3_i)^2_{jj} + \delta^2_i} - (\lambda^3_i)_{jj}],$$

the additional artificial dissipation operator is given by

$$\overline{D}^3_{ad} = P^{-1}\sum_{i=1}^{2}[D_1^i](\Lambda_i^3)[D_1^i]^T.$$

The resulting energy stable scheme is obtained by adding the additional dissipation term to the corresponding conventional WENO scheme as

$$\overline{D}^3 = D^3 + \overline{D}^3_{ad}.$$

A.3. Seventh- and eighth-order ESWENO schemes

Based on Eq. (13), $\hat{f}_{j+\frac{1}{2}}$ defined for a family of seventh-order WENO schemes is

$$\hat{f}_{j+\frac{1}{2}} = w^{LL}_{j+1/2}f^{LL}_{j+1/2} + w^{L}_{j+1/2}f^{L}_{j+1/2} + w^{C}_{j+1/2}f^{C}_{j+1/2} + w^{R}_{j+1/2}f^{R}_{j+1/2} + w^{RR}_{j+1/2}f^{RR}_{j+1/2}, \tag{97}$$

where $w^{LL}w^{L}, w^{C}$, w^{R}, and w^{RR} are weight functions assigned to each respective stencil, and are given by Eqs. (58) and (59) with

$$\tau_7 = \begin{cases} (f_{j-3} - 7f_{j-2} + 21f_{j-1} - 35f_j + 35f_{j+1} - 21f_{j+2} + 7f_{j+3} - f_{j+4})^2, & \text{for } \varphi \neq 0 \\ (-f_{j-3} + 6f_{j-2} - 15f_{j-1} + 20f_j - 15f_{j+1} + 6f_{j+2} - f_{j+3})^2, & \text{for } \varphi = 0. \end{cases}$$

The fourth-order linear fluxes $f^{(r)}_{j+1/2}$ for $r = \{LL, L, C, R, RR\}$, which are used in Eq. (97), are defined as

$$\begin{pmatrix} f^{LL}(u_{j+1/2}) \\ f^{L}(u_{j+1/2}) \\ f^{C}(u_{j+1/2}) \\ f^{R}(u_{j+1/2}) \\ f^{RR}(u_{j+1/2}) \end{pmatrix} = \frac{1}{12}\begin{pmatrix} -3 & 13 & -23 & 25 & 0 & 0 & 0 & 0 \\ 0 & 1 & -5 & 13 & 3 & 0 & 0 & 0 \\ 0 & 0 & -1 & 7 & 7 & -1 & 0 & 0 \\ 0 & 0 & 0 & 3 & 13 & -5 & 1 & 0 \\ 0 & 0 & 0 & 0 & 25 & -23 & 13 & -3 \end{pmatrix}\begin{pmatrix} f(u_{j-3}) \\ f(u_{j-2}) \\ f(u_{j-1}) \\ f(u_j) \\ f(u_{j+1}) \\ f(u_{j+2}) \\ f(u_{j+3}) \\ f(u_{j+4}) \end{pmatrix}. \tag{98}$$

The derivative matrix D^7 is now decomposed into symmetric and skew-symmetric parts as

$$D^7 = D^7_{skew} + D^7_{sym}.$$

As with the fifth-order case, the skew-symmetric component of D^7 takes the form

$$D^7_{skew} = P^{-1}Q_7; \quad Q_7 + Q_7^T = 0; \quad P = \Delta x I.$$

The scheme is seventh-order accurate if the weights are equal to their preferred values

$$d^{LL}_{\cdot} = \frac{1}{35} - \varphi, \quad d^{L}_{\cdot} = \frac{12}{35} - 8\varphi, \quad d^{C}_{\cdot} = \frac{18}{35}, \quad d^{R}_{\cdot} = \frac{4}{35} + 8\varphi, \quad d^{RR}_{\cdot} = \varphi \tag{99}$$

and eighth-order accurate for the specific value $\varphi_c = \frac{1}{70}$.

The D^7_{sym} is expressed as

$$D^7_{sym} = P^{-1}\left(D_1^4\Lambda_4^7[D_1^4]^T + D_1^3\Lambda_3^7[D_1^3]^T + D_1^2\Lambda_2^7[D_1^2]^T + D_1^1\Lambda_1^7[D_1^1]^T + D_1^0\Lambda_0^7[D_1^0]^T\right), \tag{100}$$

where $\Lambda^7_{\cdot}$ is a diagonal matrix with expressions for the jth element defined by

$$(\lambda_4^7)_{jj} = \frac{1}{8}\left[w^{LL}_{j+7/2} - w^{RR}_{j+1/2}\right], \tag{101}$$

$$(\lambda_3^7)_{jj} = \frac{1}{24}\left[w^{LL}_{j+5/2} - 9w^{LL}_{j+7/2} + w^{L}_{j+5/2} - w^{R}_{j+1/2} + 9w^{RR}_{j-1/2} - w^{RR}_{j+1/2}\right], \tag{102}$$

$$\begin{aligned}(\lambda_2^7)_{jj} = \frac{1}{24}\Big[&2w^{LL}_{j+3/2} - 11w^{LL}_{j+5/2} + 9w^{LL}_{j+7/2} + 2w^{L}_{j+3/2} - 2w^{L}_{j+5/2} \\ &- w^{C}_{j+1/2} + w^{C}_{j+3/2} + 2w^{R}_{j-1/2} - 2w^{R}_{j+1/2} - 9w^{RR}_{j-3/2} + 11w^{RR}_{j-1/2} - 2w^{RR}_{j+1/2}\Big],\end{aligned} \tag{103}$$

$$\begin{aligned}(\lambda_1^7)_{jj} = \frac{1}{24}\Big[&6w^{LL}_{i+1/2} - 13w^{LL}_{i+3/2} + 10w^{LL}_{i+5/2} - 3w^{LL}_{i+7/2} + 3w^{L}_{i+1/2} - 4w^{L}_{i+3/2} + w^{L}_{i+5/2} \\ &+ w^{C}_{i-1/2} - w^{C}_{i+3/2} - w^{R}_{i-3/2} + 4w^{R}_{i-1/2} - 3w^{R}_{i+1/2} + 3w^{RR}_{i-5/2} - 10w^{RR}_{i-3/2} + 13w^{RR}_{i-1/2} - 6w^{RR}_{i+1/2}\Big],\end{aligned} \tag{104}$$

$$(\lambda_0^7)_{jj} = \frac{1}{2}\left[-w^{LL}_{i-1/2} - w^{L}_{i-1/2} - w^{C}_{i-1/2} - w^{R}_{i-1/2} - w^{RR}_{i-1/2} + w^{LL}_{i+1/2} + w^{L}_{i+1/2} + w^{C}_{i+1/2} + w^{R}_{i+1/2} + w^{RR}_{i+1/2}\right] = 0. \tag{105}$$

Defining $(\bar{\lambda}_i^7)_{j,j}, i = \overline{1,4}$ to be smoothly positive

$$(\bar{\lambda}_i^7)_{j,j} = \frac{1}{2}\left[\sqrt{(\lambda_i^7)_{j,j}^2 + \delta_i^2} - (\lambda_i^7)_{j,j}\right],$$

the additional artificial dissipation operator is given by

$$\overline{D}_{ad}^7 = P^{-1}\sum_{i=1}^{4}[D_1^i](\bar{\Lambda}_i^7)[D_1^i]^T.$$

The resulting energy stable scheme is obtained by adding the additional dissipation term to the corresponding conventional WENO scheme as

$$\overline{D}^7 = D^7 + \overline{D}_{ad}^7.$$

References

[1] N.K. Yamaleev, M.H. Carpenter, Third-order energy stable WENO scheme, J. Comput. Phys. 228 (2009) 3025–3047.
[2] G. Jiang, C.-W. Shu, Efficient implementation of weighted ENO schemes, J. Comput. Phys. 126 (1996) 202–228.
[3] G. Jiang, S.-H. Yu, Discrete shocks for finite difference approximations to scalar conservation laws, SIAM J. Numer. Anal. 35 (2) (1998) 749.
[4] R. Ferretti, Convergence of semi-Lagrangian approximations to convex Hamilton–Jacobi equations under (very) large Courant numbers, SIAM J. Numer. Anal. 40 (6) (2003) 2240–2253.
[5] J.-M. Qiu, C.-W. Shu, Convergence of Godunov-type schemes for scalar conservation laws under large time steps, SIAM J. Numer. Anal. 46 (2008) 2211–2237.
[6] X.-D. Liu, S. Osher, T. Chan, Weighted essentially non-oscillatory schemes, J. Comput. Phys. 115 (1994) 200–212.
[7] Z.J. Wang, R.F. Chen, Optimized weighted essentially nonoscillatory schemes for linear waves with discontinuity, J. Comput. Phys. 174 (2001) 381–404.
[8] M.P. Martin, E.M. Taylor, M. Wu, V.G. Weris, A bandwidth-optimized WENO scheme for the effective direct numerical simulation of compressible turbulence, J. Comput. Phys. 220 (2006) 270–289.
[9] A.K. Henrick, T.D. Aslam, J.M. Powers, Mapped weighted essentially non-oscillatory schemes: achieving optimal order near critical points, J. Comput. Phys. 207 (2005) 542–567.
[10] R. Borges, M. Carmona, B. Costa, W.S. Don, An improved weighted essentially non-oscillatory scheme for hyperbolic conservation laws, J. Comput. Phys. 227 (2008) 3191–3211.
[11] M.H. Carpenter, J. Nordström, D. Gottlieb, A stable and conservative interface treatment of arbitrary spatial accuracy, J. Comput. Phys. 148 (1999) 341–365.
[12] H.O. Kreiss, G. Scherer, Finite Element and Finite Difference Methods for Hyperbolic Partial Differential Equations, Mathematical Aspects of Finite Elements in Partial Differential Equations, Academic Press, New York, 1974.
[13] B. Strand, Summation by parts for finite difference approximations for d/dx, J. Comput. Phys. 110 (1) (1994) 47.
[14] C.-W. Shu, Total-variation-diminishing time discretizations, SIAM J. Sci. Stat. Comput. 9 (1988) 1073.
[15] C.A. Kennedy, M.H. Carpenter, R. Lewis, Low-storage, explicit Runge–Kutta schemes for the compressible Navier–Stokes equations, Appl. Numer. Math. 35 (3) (2000) 177–219.